CIRCULAR WAVEGUIDE TAPERS FOR HIGH RESOLUTION TERAHERTZ SPECTROSCOPY

By

ALISHA SHUTLER

Bachelor of Science in Electrical Engineering

Oklahoma State University

Stillwater, OK

2009

Submitted to the Faculty of the
Graduate College of the
Oklahoma State University
in partial fulfillment of
the requirements for
the Degree of
MASTER OF SCIENCE
July 29, 2016

CIRCULAR WAVEGUIDE TAPERS FOR HIGH RESOLUTION TERAHERTZ SPECTROSCOPY

Thesis Approved By:

Dr. Dan Grischkowsky

Thesis Adviser

Dr. Weili Zhang

Dr. Jim West

.

ACKNOWLEDGEMENTS

To my husband, who believes in me always

ABSTRACT

Name: ALISHA SHUTLER

Date of Degree: JULY 29, 2016

Title of Study: CIRCULAR WAVEGUIDE TAPERS FOR HIGH RESOLUTION TERAHERTZ SPECTROSCOPY

Major Field: ELECTRICAL ENGINEERING

Parallel-plate waveguides have shown their usefulness in regards to terahertz applications by greatly enhancing the ease and sensitivity at which spectroscopic measurements of molecular samples are made. However, coupling into these devices has been a challenge, and up until now has primarily relied on the quasi-optical method of placing high resistivity silicon lenses on the outsides of the waveguide. These lenses limit the scan length of the measurements and hence, the spectral resolution. They also introduce limits with regards to reproducibility, since aligning them to the parallel plate entrance/exit points presents an additional challenge. This work explores incorporating a horn-like coupling structure onto the plates themselves, creating a cylindrically-based method of coupling with no external or moving parts. This coupling is shown to be gap-independent, on the order of the quasi-optic method, and increases the length of the scans because it removes the reflections formerly caused by the silicon lenses. For spectroscopy applications this can theoretically enhance the resonance features of molecular samples. This also has good implications for the future of terahertz science, as it presents a mechanism by which terahertz radiation can be transmitted in a gap-independent, dispersionless fashion.

TABLE OF CONTENTS

LIST OF TABLES

LIST OF FIGURES

1. INTRODUCTION

1.1 Background

In the 1980s, Bell Labs pioneered the generation and detection of terahertz (THz) waves – the relatively unused band of frequencies that lie in-between radio waves and visible light. At the time, the applications of this part of the spectrum were not implicit, and the creation and detection of these waves was difficult to do. With no driving purpose behind the technology, further development into terahertz technologies was of little interest to the optical or microwave communities. Later, when it was discovered that THz could be particularly useful in spectroscopic applications – THz waves excite molecular vibrations that give unique spectral information about the inter- and intra-molecular structures of molecules in a non-invasive, non-degenerative manner – interest exploded. Development began on the systems needed to produce high-resolution spectral information. The past three decades has since advanced THz spectroscopy considerably. In conjunction with time-domain spectroscopy (TDS), THz-TDS has proven to give unique insight into the building blocks of various molecules and compounds. The implementation of waveguides as a spectroscopic tool has been particularly useful in this regard, as it has further enhanced the resolution of the spectroscopic readings by increasing wave-molecule interactions and allowing for smaller, but better ordered samples. Integrating these waveguides into THz-TDS systems borrows techniques from both microwaves and traditional optics. This has led to an array of unique quasi-optical solutions for the implementation of guided-wave THz.

1.2 Scope of this work

This work explores recent developments in the coupling techniques used to couple THz time-domain signals into parallel-plate waveguides. Past work has introduced what is now the common method of coupling, known as the quasi-optical approach, using silicon lenses paired to parallel-plate waveguides to couple in radiation. This technique yields coupling efficiencies as high as 24%, but alignment of the lenses is laborious and can cause difficulties in obtaining reproducible data. Additionally, the high refractive index of silicon causes reflections that appear in the THz signal, thus limiting scan length and subsequently, spectral resolution. A solution was needed to introduce a coupling mechanism that could replicate the coupling strength of the quasi-optical system while eliminating the lens reflections. The solution involved drawing, once again, on the field of microwave systems. Horn antennas are structures that have been used to couple waves from one method of guided wave propagation to another, or even out to the atmosphere. They are structures that impedance match between the two modes of propagation, creating a virtually lossless method of coupling. Here, we incorporate a variation on the horn antenna structure directly onto the plates of the parallel-plate waveguide, creating an all-inclusive structure that couples and guides THz waves without the use of additional lenses or optics. Without lens reflections, these new waveguides increase the scan length of the system, thereby increasing the potential spectral resolution of molecular samples. The removal of outside components also enhances data reproducibility and increases the ease of use of these waveguides in spectroscopy.

2. THZ-TDS BASICS

This chapter describes the THz-TDS system that has now become standard in research labs. This system relies on the gating of biased photoconductive lines to both generate and detect THz pulses. The system is set up in a "4f" confocal configuration (4f for the four focal points within the system) so as the diffraction limited beams can be precisely focused between the transmitter and receiver chips, yielding exceptionally tight coupling while preserving the sub-picosecond time dependence of the source [1].The general operating principle of the system is to pass a single cycle THz pulse through a given material or structure under test. By applying a Fourier transform to the measured pulse and then comparing this to a reference pulse, taken by sending an unperturbed, freely propagating pulse through the system, a transfer function can be obtained. This function reveals the sample material's spectral response (its THz "fingerprint"), giving information on its absorption, index, and chemical content.

2.1 Background

As shown in Figure 1, there are several key components that are needed in order to create a fully operational standard THz-TDS system. These include an ultrafast laser source, transmitter and receiver chips, focusing, collimating, and beam steering optics, a frequency chopper, a lock-in amplifier, a voltage source, and a photodetector. Some components, like the frequency chopper, lock-in amp, voltage source and photodetector are standard laboratory components that are easily sourced. Other components, such as the ultrafast laser and THz transmitter and receiver chips, are unique to the application and development of THz pulse generation and detection, and are described in the following sections.

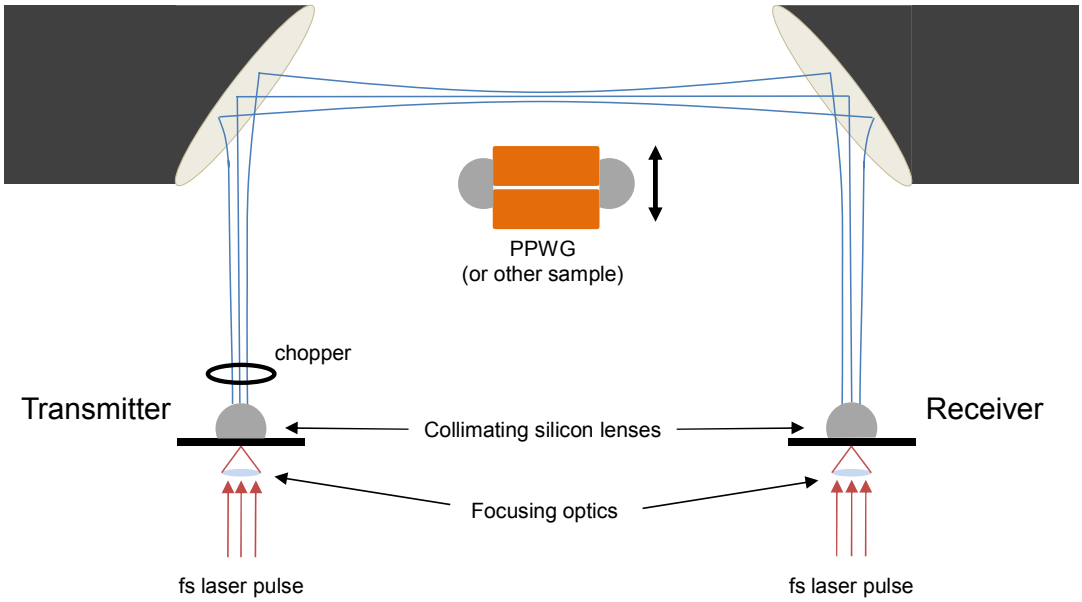

Figure 1: Layout of the standard THz-TDS system

2.2 Ultrafast laser system

In order for the transmitter and receiver chips to emit THz radiation, they must be gated by pulses from an ultrafast, femtosecond laser. This laser is composed of two primary components: a pump laser, and the femtosecond system itself. The pump feeds several Watts of continuous wave (CW) power to the ultrafast laser cavity, which in turn is mode locked and emits short, ultrafast pulses of radiation. The pump, a Millennia V system from Spectra Physics, is a diode-pumped frequency-doubled neodymium- doped (with Nd^{3+} ions) yttrium vanadate ($Nd:YVO_4$) continuous wave laser, and can provide up to 5 W of CW power at 532 nm. Optimal behavior for the femtosecond laser was found using pump powers of around 4 to 4.5 W, so the pump was set to operate within that range. The femtosecond laser is a Ti:sapph (Titatnium:sapphire or $Ti:Al_2O_3$) laser handbuilt from a Kapteyn Murnane Laboratories kit. It uses Kerr-lens mode locking to generate the 800 nm wavelength from the pump laser. A prism compressor is used inside the Ti:sapph cavity to ensure short pulses by compensating for any dispersion. The Ti:sapph laser

emits radiation of approximately 1 W at 800 nm, with pulses around 100 fs wide and a repetition rate between 80 – 100 MHz.

2.3 Gating the photoconductive switches

Once the ultrafast beam is produced, it must then be delivered to the two photoconductive switches that comprise the transmitter and receiver chips. The chips are gated properly when the beam excites the dipole on the transmitter chip, resulting in THz radiation which then strikes the receiver chip at the same time that the receiver chip is gated by another optical pulse. In order to do this, an optical beamsplitter is used on the incoming ultrafast radiation, dividing the laser pulse into two and sending each smaller pulse along its own path: one pulse for the transmitter chip, and one pulse for the receiver chip. The optical path lengths of both these new pulses are adjusted to match each other as much as possible (the optical path length for the transmitter side beam must include the additional distance from the transmitter chip to the receiver chip in order to allow for the THz propagation to the receiver chip). A scanning delay line placed along one of the optical paths aids in this. The opposite path is adjusted to compensate for the increased distance of the delay line, but the scanning line allows the user to scan along until the resulting THz signal (from having each path length exactly equal) is found. This scanning delay line is also the tool that also allows information to be read from a single-shot THz pulse cycle (see following section).

It is interesting to note that it is possible to get accurate THz information using two different ultrafast pulses, as long as the differences in time between the pulses are multiples of each other. However, this method is extremely uncommon and is typically only used when long THz path lengths (between the transmitter and receiver pairs) are required [2].

2.4 Photoconductive dipole antennas

The basic transmitter structure consists of a pair of photoconductive lines, creating a Hertzian dipole antenna that radiates once the laser pulse strikes the transmission lines. As seen in Figure 2, the excitation beam strikes high on the transmitter line pairs, near the positive bias, to generate a stronger THz signal due to the faster acceleration of free carriers. On the receiver side, a bias is produced across the metal lines by the incoming THz beam. The optical laser beam then acts as a bridge between the top and bottom metal lines, causing free carriers to accelerate. The resulting current is measureable by an amplifier. This process is described in greater detail in this section.

For the transmitter, the lines have a positively charged bias placed across them (the optimal operating potential varies and is based upon the substrate, structure, and width of the lines, and can be anywhere from 50V to 70V for coplanar lines) and as the femtosecond laser strikes upon the metal-semiconductor edge of the positively-biased line, it creates a spot of photocarriers in a region of extremely high electric field. The acceleration of these carriers causes a release of energy in the form of THz radiation. The pulses on the antenna from the ultrafast laser produce synchronous bursts of radiation, which are largely emitted into the GaAs substructure normal to the surface and are then collimated by a high resistivity silicon lens with optical contact onto the direct backside of the chip. This process, viewed from a more electromagnetic point of view, is simply the creation of an induced electromagnetic field from the flow of current the laser pulse produces. The width of the lines and their separation determines the THz response. Smaller dipoles create weaker, broader THz pulses, while the reverse is true for larger spaced dipoles. A typical configuration for these lines is known as 10-80-10, where 10 μm-wide metallic electrodes are separated by 80 μm on the GaAs substrate. The incoming optical beam is typically regulated (via optical attenuator) to strike the transmission lines with only 5-15 mW of optical CW power; in conjunction with the applied voltage, this produces currents of around 2-3 mA DC. Higher

voltages and higher optical powers are typically not desired, as they quickly yield diminishing returns – noise levels increase, and the lifetime of the eletrodes descrease as the surface deposited metals slowly degenerate.

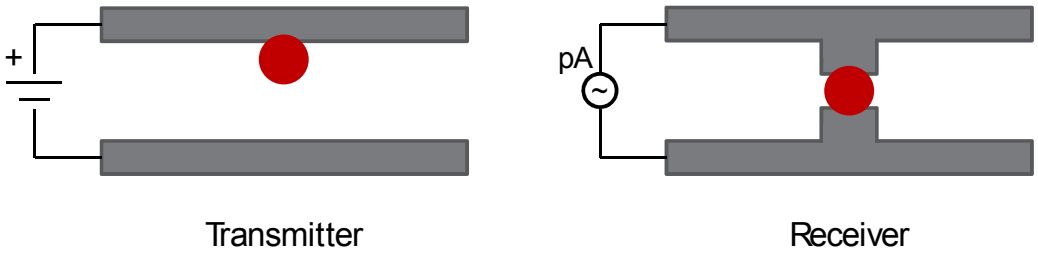

Figure 2: Transmitter (left) and receiver (right) photoconductive switches (PCSs). The red dot indicates the incoming excitation beam from the optical ultrafast laser source.

As the THz radiation propagates, it is captured and collimated by the 4f confocal system and then refocused onto the hemispherical silicon lens on the backside of the receiver chip. As the focused radiation pulse hits the detector, a transient voltage appears across the gap. The induced voltage is measured by shorting the gap with the 80 fs laser pulses in the detection beam and measuring the collected charge vs the time delay between the excitation and detection laser pulses. This is why it is crucial that the laser pulse strike the receiver line pair at the same time as the THz pulse strikes from the transmitter – if the two pulses are mismatched in time, no photocurrent will be generated and the signal will not be read. As the laser and THz pulse both strike the photoconductive lines on the receiver, a photocurrent is generated and fed through a current amplifier. This current is what is read by the computer when collecting data from the THz pulses. Rather than using GaAs, the receiver chips are usually composed of oxygen-implanted silicon-on-sapphire (SOS). The THz current is only measurable during the response time of the carriers in the SOS after illumination [1]. The current is proportional to the incident THz field on the dipole.

By varying the time of arrival between the optical excitation beam on the transmitter and optical detection beam on the receiver via changing the path length on the given delay arm, the electric field of the THz pulse impinging on the dipole induces a current that can be measured. This current is proportional to the field and will represent the pulse shape if the relaxation time of the detector is sufficiently short. For the purposes of this work, a gating pulse of 100 fs or less is suitable to resolve a THz pulse on the order of picoseconds in duration.

2.5 Capturing THz radiation

Once the THz radiation is generated on the transmitter, it is emitted outward in an expanding spherical wave from the point of laser excitation normal to the backside surface of the GaAs chip (see Figure 3). This is an inherent feature of dipoles emitting radiation in the near-field – most of the radiated power is emitted into the dielectric and only very little is radiated out into the air. For Hertzian dipoles (point sources) with dimensions small compared to any of the radiated wavelengths, the emitted radiation can be collimated using optical techniques. To capture this radiation and collimate it to the system, a hemispherical silicon lens is placed in optical contact on the backside of the GaAs transmitter. The silicon lens has been cut and flattened out on one side of the hemisphere. Hence, both diameter and height are needed to fully describe the physical properties of the collimating lens (see Figure 3). Typical dimensions are around 6 mm height and 10 mm diameter. A Gaussian intensity profile is assumed with constant phase across the aperture formed by the silicon lens. The beam expands according to standard diffraction theory.

2.6 Collimating the THz beam

The THz beams generated by the photoconductive chips can be accurately modeled using Gaussian Beam theory [3]. If we assume Gaussian beams, we can arrange the final THz system in such a way as to maximize signal amplitude and bandwidth. It is desirable to have a THz system with room to place sample structures and materials for analysis. By creating a confocal system,

lenses can be chosen and placed at such distances so as to maintain a unity power transfer function between the transmitter and receiver side, with the desired operating distances between the transmitter and receiver chips. By selecting parabaloidal mirrors with equal focal lengths and placing them a focal distance away from the transmitter and receiver, and two focal lengths away from each other, a 4 f system is created. This system has a unity optical transfer function and maximizes signal amplitude and bandwidth. Typically, focal lengths of 119 mm are used for the off-axis parabaloidal mirrors, giving a total propagation range of around less than 50 cm. These mirrors integrate over the entire face of the beam. Improper alignment can drastically reduce the spectral response. The receiver mirror redirects and refocuses the THz beam onto the backside of the receiver chip. The beamwaist at the center between the two parabaloidal mirrors is frequency dependent and, due to the broad system bandwidth, typically ranges in diameter from 9 mm (at 0.5 THz) to 1 mm (at 4 THz).

(A)

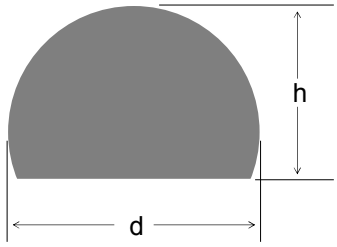

(B)

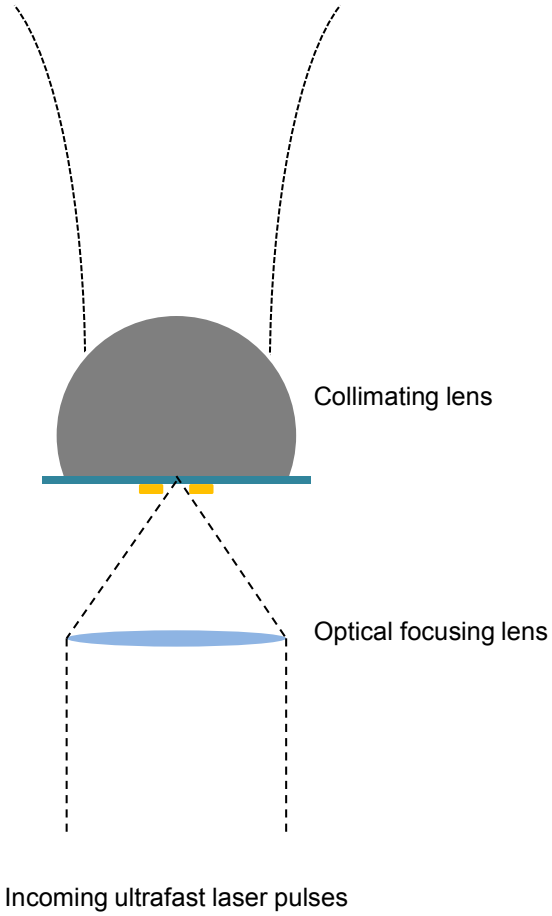

Figure 3: (A) Truncated spherical silicon lens with dimensions length (L) x height (h) x diameter (d). (B) Shows the truncated spherical lens placed on the backside of the THz transmitter/receiver chips. The radiation generated by the PCS is collected by the silicon lens and collimated out to the rest of the system.

2.7 System electronics

2.7.1. Optical chopper/lock-in detector

The current is measured on the receiver chip using a current amplifier feeding into a lock-in detector. The detector is frequency locked-to an optical chopper that is used to modulate the THz signal in a square-wave (as long as the blades of the chopper are large enough, this approximation is valid). The optical chopper is placed near the transmitter lens and set to spin a known frequency. This frequency is fed to the lock-in detector as the detector's reference signal. By taking the difference frequency between this reference and the modulation, a DC signal is measured.

2.7.2 Scanning delay line

A retroreflector is mounted on a motion controlled scanning delay line. This provides the delay between the optical pump and probe beams (the beams that strike the transmitter and receiver chips) in order to fully resolve the THz signal. The step size of the motion determines the total length of the time scan, and hence, the spectral resolution:

$$\Delta\nu = \frac{1}{N\Delta t} \tag{1}$$

where $\Delta\nu$ is the spectral width, N is the number of steps, and Δt is the time step per data point. The time steps are determined by the spatial movement of the delay line between current measurements, keeping in mind that the optical path introduced by the delay line is doubled (because of the retroreflector).

3. HIGH RESOLUTION THZ-TDS USING PARALLEL-PLATE WAVEGUIDES

Prior to the development of THz-TDS, FTIR (Fourier transform infrared spectroscopy) was used to extract the vibrational information of molecular samples that exhibit characteristic resonant frequencies in the THz frequency range and molecular transitions in the meV energy range. But this technique was plagued by poor performance of both the sources and detectors. It was not until the femtosecond laser was introduced that the development of optical excitation of photoconductive transmitters and receivers was developed. This allowed scientists to construct THz spectrometer systems with signal-to-noise ratios as high as 10,000:1 [1] in the same frequency spectrum. Using these systems, a number of samples and sample states can be analyzed.

The nature of the sample influences the nature of the spectroscopic data. Gas samples exhibit sharp spectral features with their associated vibrational modes. Liquids tend to have much broader features: non-polar liquids only weakly absorb THz, while highly-polar liquids (such as water) tend to exhibit such strong interactions as to feature broadband absorption across the entire THz spectrum [4]. Solid state samples, on the other hand, exhibit absorption responses that are almost entirely dependent on the crystallinity of the sample. The more crystalline, the sharper the absorption features; the more amorphous a sample, the more broadband the spectral response.

Several mechanisms have been introduced in order to gain as high a spectral sensitivity as possible when working with solid state samples. These include the use of sub-wavelength confinement of the THz beam with the sample in question. By confining the beam to sub-

wavelengths, the beam is forced to interact strongly with the sample, thereby enhancing the spectral strength of the resonant absorption. Parallel-plate waveguides have found a niche use in this regard. They can confine the THz beam down to sub-wavelengths in an almost dispersion-less fashion without causing significant absorption losses. This development is a much welcomed improvement over the previous standard of solid state spectroscopy, where single-crystals or diluted pellets of crystalline material were used for analysis. The single crystals were difficult to grow, if at all possible, and while they gave excellent structural information, they absorbed radiation too well, causing spectral features that were so strong as to be unusable. Therefore, they had to be grown so thin that they did not allow for such strong interactions; however, the thin crystals caused reflections in the THz signal, thereby limiting scan length and hence, spectral resolution. The polycrystalline pellets, on the other hand, were easy to produce and modify to thickness. However, the random alignment of the microcrystals within the pellets produced significant, broad, inhomogeneous broadening. In addition, the high pressure required to form the pellets broke down the crystalline structure, causing defects. The pellets were also subject to the same Fresnel reflection losses as the thin single-crystals, yet again limiting scan length and spectral resolution.

When it was demonstrated that THz waves could be guided in a sub-wavelength fashion over long propagating distances using dispersionless, two conductor waveguides [5], it wasn't long before the waveguides quickly found use in applied spectroscopy. It was found that small amounts of crystalline samples could be deposited directly onto the surface of the waveguide. With only μg of sample present, the high spatial confinement of the parallel-plate waveguide was able to help resolve very narrow spectral features of the microcrystalline sample [6]. By varying deposition methods, it was also found that it was possible to deposit more uniform layers of sample, yielding more accurate information about sample thickness, crystalline orientation, and vibrational structure. The additional spectroscopic method of cooling both the waveguide and

sample down to liquid nitrogen temperatures (~77K) or even lower (~10K) using cryogenic methods reduced thermal broadening and improved the conductivity of the waveguides, further enhancing spectral resolutions [7]. With the success of these experiments, waveguide THz-TDS was found to be a viable solution to some important problems of far-infrared spectroscopy.

The previous work with parallel-plate waveguides involved using a quasi-optical method of coupling radiation into and out of the waveguide [5]. The following sections describe this technique. Then, a new method is introduced which removes the optical component to create a fully self-contained parallel-plate system. The next chapter will describe this new work in more detail.

3.1 Background

Before the parallel-plate waveguide was introduced into THz-TDS, traditional, single-conductor waveguides were tested and used with mixed results. It was found that broadband coupling of THz radiation could be achieved using rectangular and cylindrical waveguides [8], plastic ribbon waveguides [9], and single crystal sapphire fibers [10]. However, all of these techniques suffered from group velocity dispersion (GVD), excessive pulse broadening, and operation only in either the TM (transverse magnetic) or TE (transverse electric) modes with an inherent cutoff frequency that became a challenge to efficient waveguide design. By contrast, two-conductor waveguides do not have these issues as they can operate in the TEM (transverse electromagnetic) mode which has no cutoff frequency [5]. The two-conductor waveguides do not suffer from GVD, and therefore, do not suffer from excessive pulse broadening. Most of the losses within the two-conductor waveguide are found within the skin-depth layer of the metal surface. Theoretically, assuming perfect conductors and perfectly flat plates, the THz pulse can be infinitely compressed between the two plates [11] [12]. Absorption is then viewed as a perturbation to the model. This model holds true as long as the absorption per unit length is much less than the wavelengths of

the pulse. As the absorption becomes on the order of the wavelengths, then the model breaks down and lumped parameter theory must be used (see Section 4.4 Gap independent conduction loss). The absorption losses are due to conductivity loss of the metal surfaces and are described in more depth in the following section. Conveniently, testing has revealed them to be low, therefore propagation of the THz pulse through the PPWG yields a near-dispersion free, near-zero distortion, low loss propagation of signal, and most modeling can be done assuming perfect conductors [12].

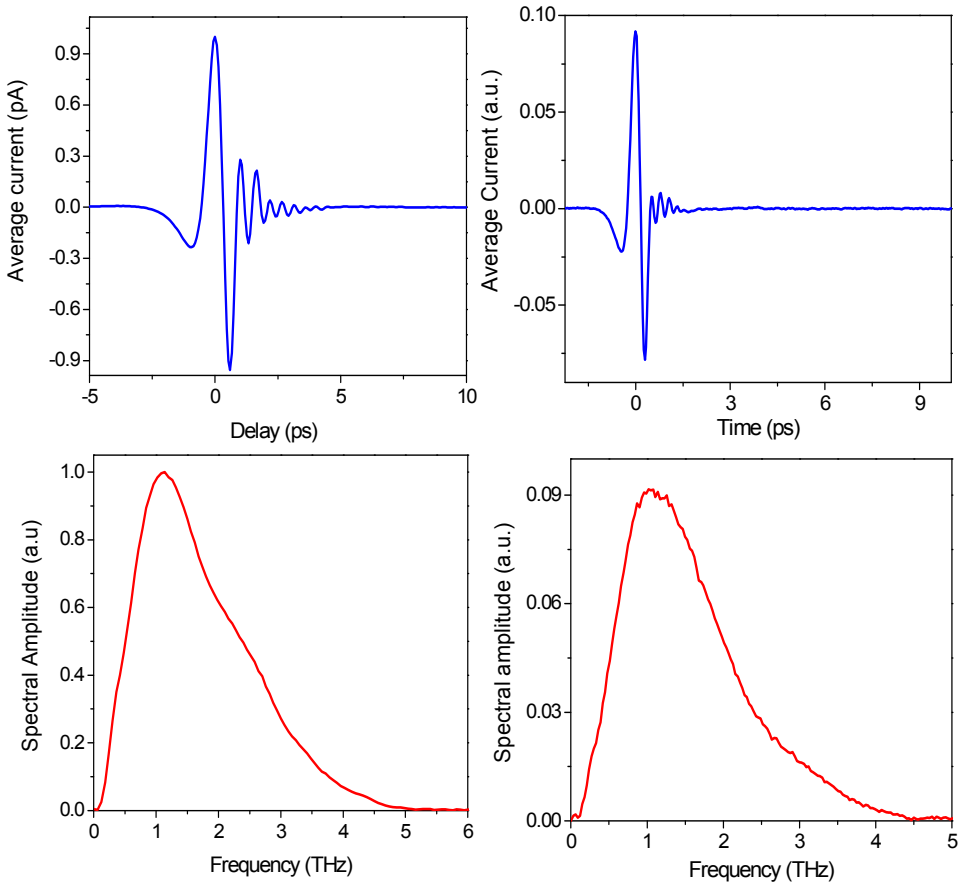

Figure 4: Two THz pulses are given here with their corresponding spectra. On the left is a THz pulse shown propagating through freespace. On the right, a THz pulse is shown propagating through two silicon lenses. Both pulses have been normalized to demonstrate that little broadening or distortion occurs [14].

In this work, I continue to use the PPWGs for THz-TDS, and focus on the challenges associated with efficient coupling into the device.

3.2 Theory of operation

The theory of operation of the parallel-plate waveguide is well known in the microwaves community. Assuming plane wave propagation, based on the two-dimensional analysis for an input electric field linearly polarized normal to the plates, only TM modes exist. With direction of propagation along the z-axis, assuming no losses [13]:

$$H_x = A_m \cos\left(\frac{m\pi}{b}y\right) e^{-j\beta_z z} \tag{2}$$

$$E_y = \frac{A_m \beta_z}{\omega_0 \varepsilon} \cos\left(\frac{m\pi}{b}y\right) e^{-j\beta_z z} \tag{3}$$

$$E_z = \frac{A_m}{j\omega_0 \varepsilon} \frac{m\pi}{b} \sin\left(\frac{m\pi}{b}y\right) e^{-j\beta_z z} \tag{4}$$

$$\beta_0 = \sqrt{\omega_0 \mu \varepsilon} = \beta_z + \left(\frac{m\pi}{b}\right) \tag{5}$$

where H_x is the magnetic field along the x-direction, E_y and E_z are the electric fields along the y- and z-directions, respectively, A_m is the field amplitude, ω is the frequency, μ and ε the permeability and permittivity, β the wavevector, b is the plate separation, y is confined between the bounds $0 \leq y \leq b$, m is the mode number where m = 1, 2, 3…, and 0 denotes a free space quantity.

Additionally, the cutoff frequency can be defined as:

$$f_{cm} = \frac{mc}{2bn_d} \tag{6}$$

where n_d is the refractive index of the medium between the two plates (in our cases, this is usually air where $n_d = 1$). Note that the lowest order operating mode of the PPWG is the TM0 mode,

which is in fact the TEM mode, which has no cutoff frequency. (Side note: this also implies that the PPWG, or two-conductor waveguide, has the unique ability to propagate even a DC signal.) Higher order modes can simply be avoided by spacing the plates apart at such a distance that the cutoff frequency for the next order mode (the TM2 mode) falls outside the input spectrum.

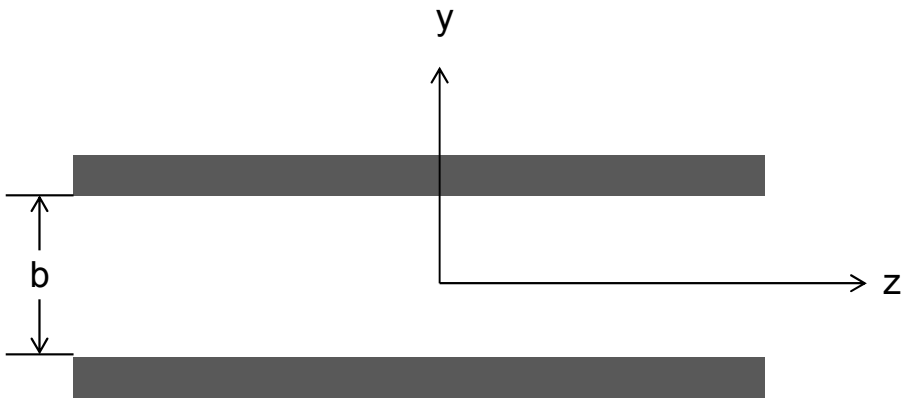

Figure 5: 2D view of the metal parallel plates and axis of propagation

In general, two kinds of losses can arise: conduction losses (due to a rise in conduction currents in the metal plates of the surface), and dielectric losses (arising from the dielectric medium between the plates). Since the PPWGs are air filled, dielectric losses can be neglected. The conduction losses can be expressed in terms of an amplitude absorption coefficient [13], [12]:

$$\alpha = \frac{R}{\eta_0 b} \tag{7}$$

where $R = 10.88 \times 10^{-3} \sqrt{\frac{10^7}{\sigma \lambda_0}}$ and is the freespace metal impedance given in terms of Ohms, σ is the conductivity in terms of Siemens per meter, η_0 is the freespace wave impedance of 377 Ω, b is the plate separation, and α is given in terms of m^{-1} (or more commonly, expressed in cm^{-1}). This equation is dependent on both the frequency of the system and the conductivity of the metal. This becomes evident when the R equation is incorporated into the equation for α, yielding:

$$\alpha_0 = 1.6662 \times 10^{-3} \left[\frac{f}{\sigma}\right]^{0.5} \left(\frac{1}{b}\right) \quad (8)$$

From the above, it is clear that the absorption has a $\sqrt{f}$ dependence and an inverse proportionality to b. It might seem possible to reduce the absorption losses without bound by increasing b, but as the plate separation increases, more higher-order modes come into play, thereby limiting the separation. Therefore, there is a distinct tradeoff when optimizing waveguide design between achieving single mode propagation while minimizing conduction losses.

3.3 Challenges with coupling

The biggest challenge in using the PPWG comes with the coupling radiation into and out of the guide. How do you efficiently couple radiation without introducing dispersion, significant losses, or other aberrations, such as reflections?

Up until now, the labs here at Oklahoma State University solved this issue by introducing a quasi-optical method of wavelength confinement. As shown in Figure 6, plano-cylindrical silicon lenses were placed at the input and output faces of the THz waveguide. Similar to the truncated spherical lenses used on the transmitter/receiver chips, the plano-cylindrical lenses were flat along the longitudinal length of the lens so that they lay flat against the PPWG. The lenses were held in place by metal holders placed outside the boundaries of the waveguide. Plastic-tip set screws in the holders were used to tighten the lenses into place as well as align them to the waveguide openings. The thickness of the silicon lenses determined the focal length of the radiation into the waveguide. The most common lens dimensions used were 15 mm (L) x 10 mm (d) x 6.56 mm (h) with a 5 mm radius of curvature. The input silicon lens focused the incoming terahertz pulse to an elliptical spot with the minor axis of 150 μm, perpendicular to the waveguide

plates, and the linearly wavelength-dependent major axis is 9 mm at 1 THz, parallel to the waveguide plates.

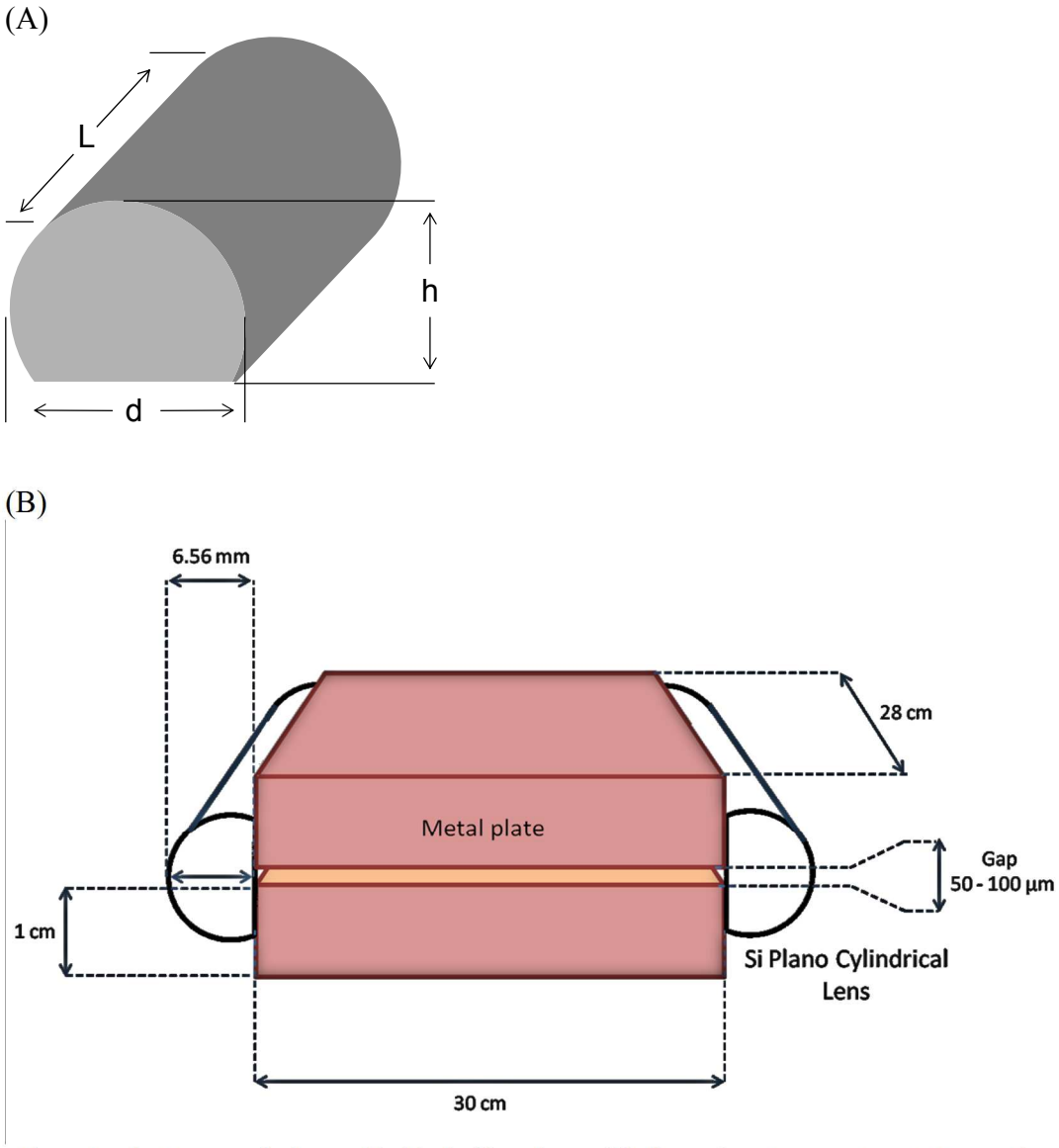

Figure 6: (A) Truncated plano-cylindrical silicon lens with dimensions 15 mm (L) x 6.56 mm (h) x 10 mm (d). (B) Demonstrates how the lenses are attached to the outside edges of the PPWG [14].

The benefit to using the silicon lenses were that they allowed the THz radiation to couple in and out of the PPWG in a near-dispersion free manner, owing to the fact that silicon introduces negligible GVD in the THz frequency range. However, Figure 7 demonstrates that the high index of refraction of the silicon (at n=3.42) also introduced significant Fresnel losses that manifested

themselves in terms of total transmission loss and the addition of reflections in the THz signal – which limited the scan length of the system and hence, the spectral resolution for a measurement.

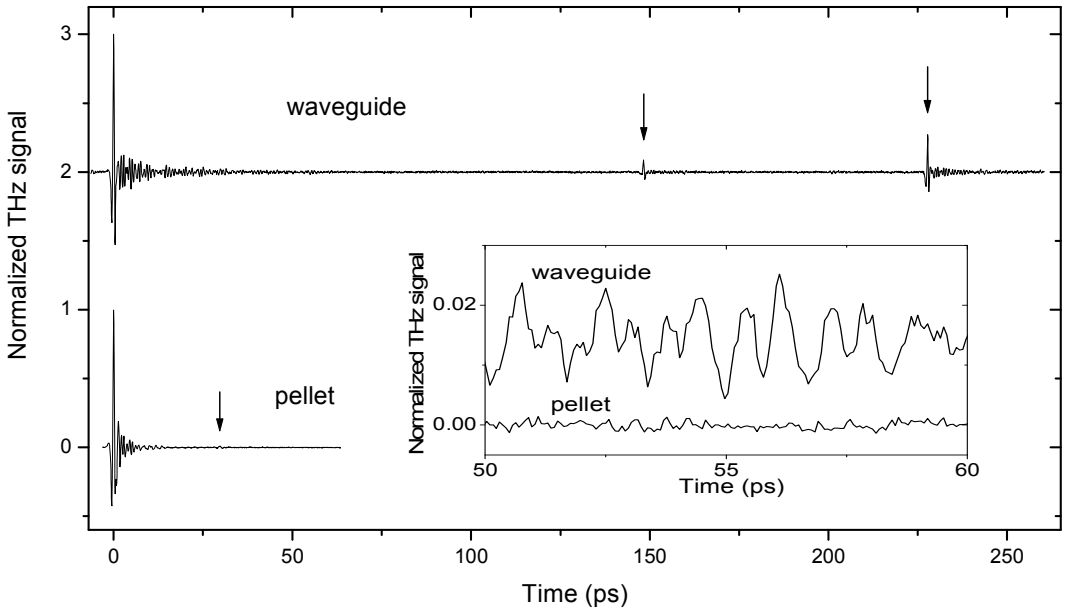

Figure 7: Extended THz pulse through a waveguide (top trace) and through a pellet (bottom trace) [7]

As seen in Figure 7, the pulse through a waveguide shows a clear reflection at 150 ps. This is due to the 6.56 mm silicon lenses used to couple the THz radiation to the PPWG. (The second reflection at 228 ps in Figure 7 is due to external, non-system silicon lenses as described in [7].) Eventually, part of the reflection will pass through the silicon lens and can be seen by scanning out over a larger period of time. The pulse delay introduced by the silicon lenses can be easily calculated from the following equation:

$$t = 2\left[(n-1)\left(\frac{h}{c}\right)\right] \tag{9}$$

where t is the time, the multiplicative factor of 2 is introduced as there are two (entrance and exit) silicon lenses, h is the thickness of the each silicon lens, c is the speed of light in freespace, and n is the index of refraction.

Although generally, silicon lenses were used with the typical lens dimensions already mentioned, initially three different thickness silicon lenses were tested and their performances were compared. The first reflection for the two 6.56 mm-thick lenses occurred 150 ps after the main pulse, limiting the instrument frequency resolution to 6.6 GHz. For two 7.07 mm lenses, this increased the delay to 161 ps after the main pulse, marginally increasing frequency resolution to 6.2 GHz. For 15 mm silicon lenses, the pulse reflection was delayed to 342 ps, increasing frequency resolution to 2.9 GHz, effectively doubling what could be achieved. However, as shown in Figure 8, each thickness lens also had dramatically different coupling ratios, which significantly altered the amplitude coupling of the THz transmission into the waveguide and hence, the signal-to-noise ratio. The 6.56 mm lenses could achieve coupling of around 24%, the 7.07 mm lenses around 18%, while the 15 mm lenses could only achieve around 9%. This meant that while the 15 mm-thick lenses could achieve the greatest system frequency resolution, the signal sensitivity was greatly reduced. The best performance-to-cost ratio was found in the 6.56 mm lenses, and this is why they were typically used for waveguide applications.

The transmission loss through the silicon lenses could be calculated using the well-known Fresnel equations for propagation through an indexed medium. With an index of n = 3.42, and propagation at normal incidence, the Fresnel losses for the combined lenses reduced the amplitude of the terahertz field by 0.49, or about 50%, where the transmission for each silicon lens is given by:

$$T = \frac{4n}{(1+n)^2} \tag{10}$$

There were other smaller, but no less important, mechanical challenges that needed to be taken into account, too. Alignment of the silicon lenses could be tricky and had to be performed manually, under a microscope and then again within the THz system itself, for both input and output lenses each time the waveguide was assembled. This method limited the reproducibility of

the guided wave system as minor changes were introduced each time the waveguide was assembled and re-assembled. The ultimate combination of these factors led my colleagues and me to seek out another method of coupling radiation into the PPWGs, one that could overcome the limitations and challenges of the silicon lenses.

(A)

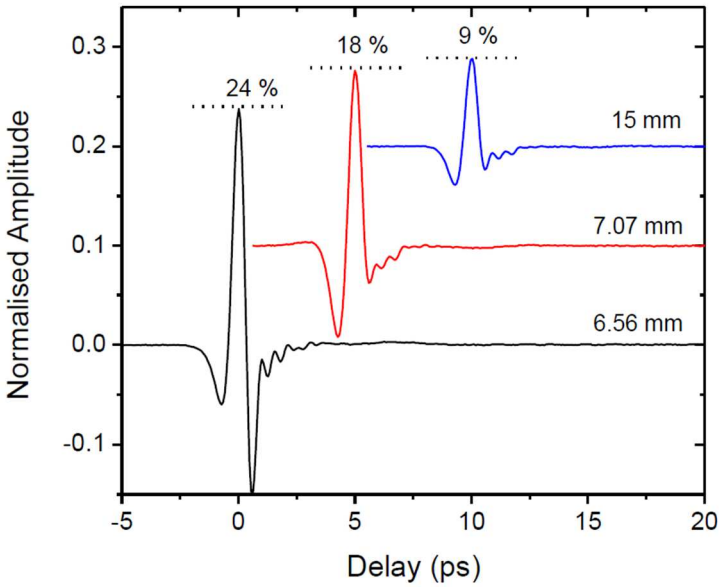

(B)

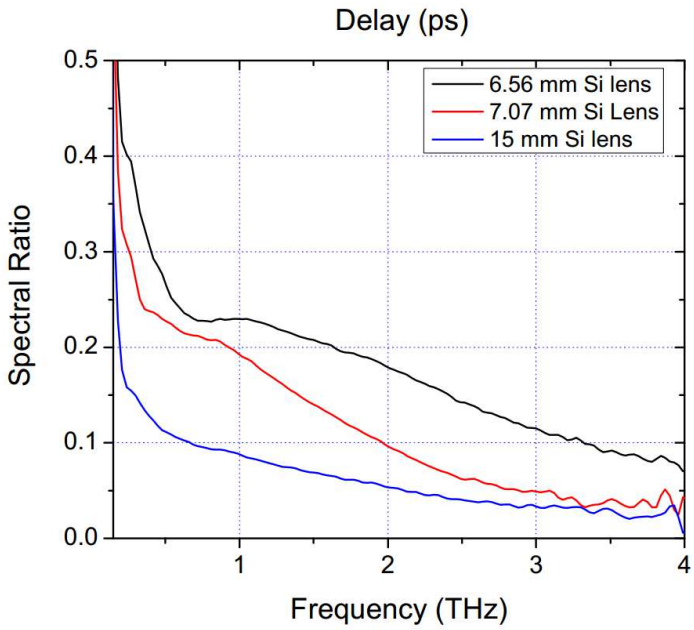

Figure 8: (A) Comparison of coupling performance of the 6.56 mm, 7.07 mm, and 15 mm thick silicon lenses [14]. (B) Demonstrates the frequency dependent coupling of each lens option [14].

3.4 Incorporating a microwaves-based approach

Horn antennas are guiding structures that typically serve as a gradual transition between two disparate media (e.g. between a waveguide and freespace or even between two parallel-plate waveguides with different gap spacing). In reality, they are essentially waveguides that feature tapered walls along either one or two dimensions. In the world of microwave design, the structure of the horn antenna is carefully designed so as to impedance match the two media the antenna is coupling radiation between. This impedance matching allows radiation to propagate in a lossless and dispersionless (or near enough) fashion.

Using horn antennas in the design of THz systems has been done before. It was notably featured as part of a THz quantum cascade laser [15], and has even been used to couple radiation into and out of parallel-plate waveguides [16]. These waveguides used carefully fabricated tapers at varying angles of taper to optimally couple radiation into the guide. Amongst the taper designs fabricated and tested, the optimal angle was found to be a mere 3° from the axis of propagation; the conclusion was drawn that with a yet more slowly varying taper, an even higher coupling ratio could be achieved. However, in order to both match both the gap opening of the PPWG and the opening required for coupling of the THz radiation (9 mm at 0.5 THz), and feature such a gentle taper angle, the taper length becomes exponentially longer as the angle decreases, creating a rather long waveguide structure for use with standard THz-TDS systems.

I decided to explore the feasibility of creating a waveguide taper (horn antenna) that coupled radiation on the order of the quasi-optical technique, but that would negate the Fresnel losses of the silicon lenses and that would not require as much material as suggested by [16]. I first began working with a colleague who explored using metal shims (thin sheets of metal that were cut down to size and were flexible enough to bend into an adiabatic, taper-like shape) as a

replacement for the silicon lens couplers. We compared various taper lengths and shapes and examined their propagation characteristics. With the knowledge gained from these results, I then designed and fabricated a series of solid metal tapers and PPWGs featuring these tapers, began testing their coupling capabilities as well as the absorption of radiation within the skin depth layer of the metal surfaces, and explored their feasibility for use with spectroscopic applications. The results of this work follow.

3.4.1 Fabrication and performance of flares crafted from metal shims

Our colleague, Dr. M. Theuer, was first inspired to try using a metal flare to couple radiation between free space and a waveguide after observing THz pulse compression using a metallic cylinder over a coated metal sheet [17]. He and his co-authors observed unprecedented compression of the THz wave on the sheet when it encountered the metal cylinder in its path. They realized that it was the adiabatically varying gap between the cylinder and sheet that was efficiently compressing the THz pulse into the sub-wavelength confinement. A literature search revealed that flares had been applied in other instances (see previous section). With that, we realized that we could potentially use a similarly varying metallic structure at the entrance to the parallel plate waveguides to enhance the coupling to the device. This structure, essentially a simplified version of a horn antenna, could be easily made using thin sheets of flexible metal and attached to the entrance and exit faces of the waveguides and the coupling could be then measured from there.

Shims are smooth, thin sheets of metal that can be purchased in rolls of several meters of length with typical thicknesses varying anywhere from 12 μm to 200 μm. The thinness of the sheets allows for a certain amount of flexibility, while the natural tensile strength of the metal allows the shim to hold a particular shape once that shape has been carefully introduced. Aluminum and copper shims with thicknesses of around 50-100 μm were used to create flared structures.

Construction of the flares was simple. Using a paper cutter, 15 mm wide strips were cut from a 9 cm diameter, 15 cm wide roll of standard commercial 100 μm thick copper or aluminum shim. The strips were then pressed and rolled flat using a metal cylinder – this ensured that the shim strips are flat and removes bends from the material.

To evaluate the coupling efficiency of the flares independent of the waveguide losses, the experimental arrangement shown in the inset in Figure 9 – B was used [18]. With this arrangement, the coupling efficiency of the flare coupler was studied as a function of flare opening as well as the minimum gap size. Two 25 mm diameter circular rods compressed the copper shims together in the center, while the gap was kept open by the mechanical spacers outside of the THz beam. At the points indicated in the figure, the cylinders were moved with the aid of a micrometer. This allowed us to control both the gap size at the center of the flares and the flare opening. The results obtained from this investigation are summarized in Figure 9 – A [19]. From this, it is clear that independent of the gap size, the best coupling ratio is obtained for an opening between 5 – 8 mm for a 15 cm long flare. In particular, for the center gap sizes we are interested in, i.e. the typical spacings of 50 and 100 μm commonly associated with PPWGs, maximum coupling ratios of 39% and 41% were obtained, respectively, using a flare opening of 6.3 mm. This coupling is almost 15% more than the maximum achieved (see Figure 8) using a 6.56 mm silicon lens. In addition to the 15 cm long flare, 8 and 12 cm flare lengths were also tested. For these flare lengths, this distance between the openings was varied from 0 degrees (point of contact) to 25 degrees while maintaining a gap spacing of 100 μm. The longer flare was found to perform better, giving 33% coupling with an opening of 15 mm. Compare this to Figure 9 – A, where a 15 cm long flare structure with a 100 μm gap can achieve coupling as high as 41%. More details can be seen in Figure 9 – B.

The results showed promise. For the two studies, the conclusion was drawn that the longer the flared structure, the better the resulting coupling that could be achieved. This was most likely due to the increased adiabaticity of the longer flares. The more gradual and smooth the transition from free space to sub-wavelength confinement, the more adiabatic the flares. The downside to the longer flares meant that ultimately, depending on the flare length selected, a flare-coupled PPWG could become quite long. A long waveguide structure could become more difficult to fit into our system. The balance between flare length and flare openings needed to be further considered when designing a flare-coupled PPWG.

(A)

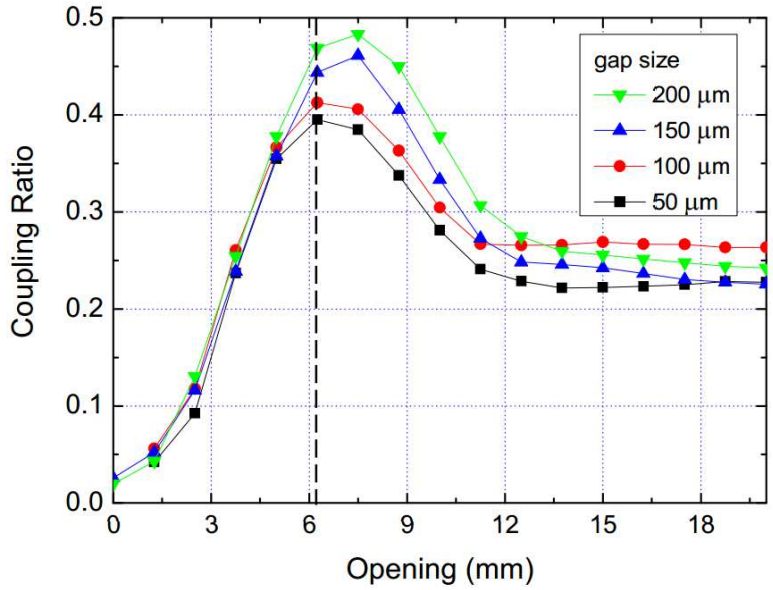

(B)

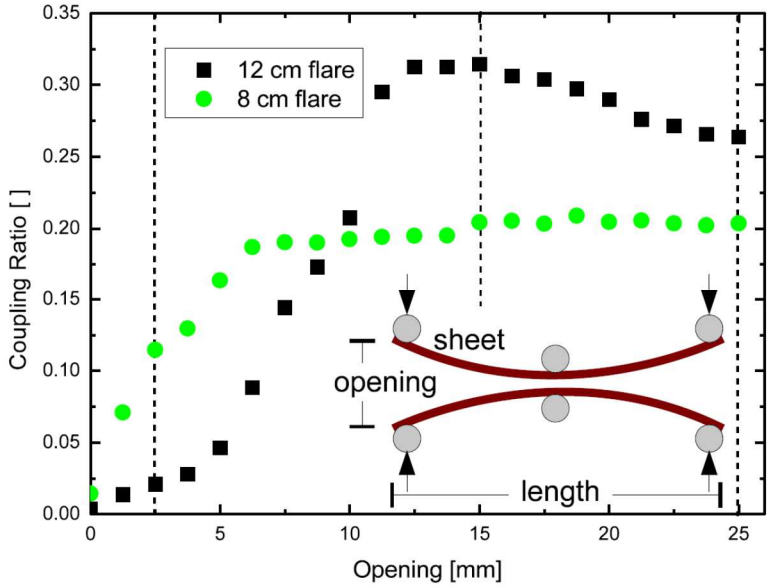

Figure 9: (A) Measured coupling ratios (defined here as amplitude transmission divided by freespace) for a flare of 15 cm length with varying gap sizes and openings [19]. (B) Comparison of the coupling for 8 and 12 cm long flares with varying opening distances, maintaining a gap size of 100 µm [18].

3.4.2 Flare-coupled parallel-plate waveguides

The next step was to implement these metallic flares onto the PPWGs and compare their coupling to the silicon lenses. By placing the 3 cm long PPWG at the center of the flare, the flare naturally flattens out in its center. The flare can be attached to the PPWG by a number of methods, either by gluing the backside of the flares onto the waveguide surface, or by taping the flares to the surface just outside the beam extent. See Figure 10: (a) The silicon-lens coupled PPWG and (b) the new flare-coupled PPWG for layout.

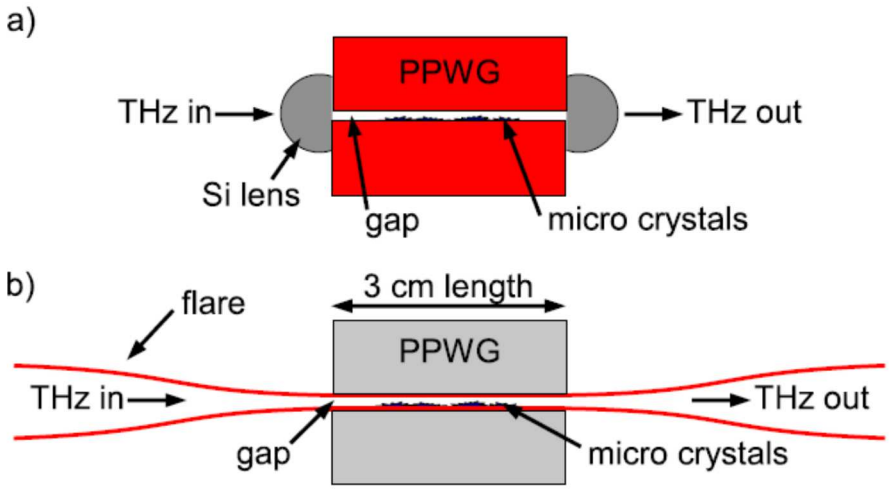

Figure 10: (a) The silicon-lens coupled PPWG and (b) the new flare-coupled PPWG [19].

By maintaining a flare opening of over 5 mm at the entrance and exit, it was found that the flare-coupled waveguides demonstrated broadband coupling performance enhancement over the silicon-lens coupled waveguide with a gap size of 50 μm, peaking with an increase of 1.6x at 1 THz (see Figure 11). Not only was there a coupling increase, but as the gap sizes became narrower, the coupling ratios did not reduce by much, varying from around 48% for a 200 μm gap to around 39% for 50 μm [19]. In addition, the system scan length for the flare-coupled PPWGs also increased, as the Fresnel reflections seen at 150 ps (for a 6.56 mm silicon lens) were no

longer there. These factors could be taken into consideration for sensitivity enhancement when experimenting with weakly absorbing samples in spectroscopic studies.

As shown in Figure 11, This study also included sample data for TCNQ, 1,2 DCB and salicylic acid. For more information, see [19]. I will not review all the data here, but the flare-coupled PPWG was showing promise as a great alternative to coupling with the traditional quasi-optical approach.

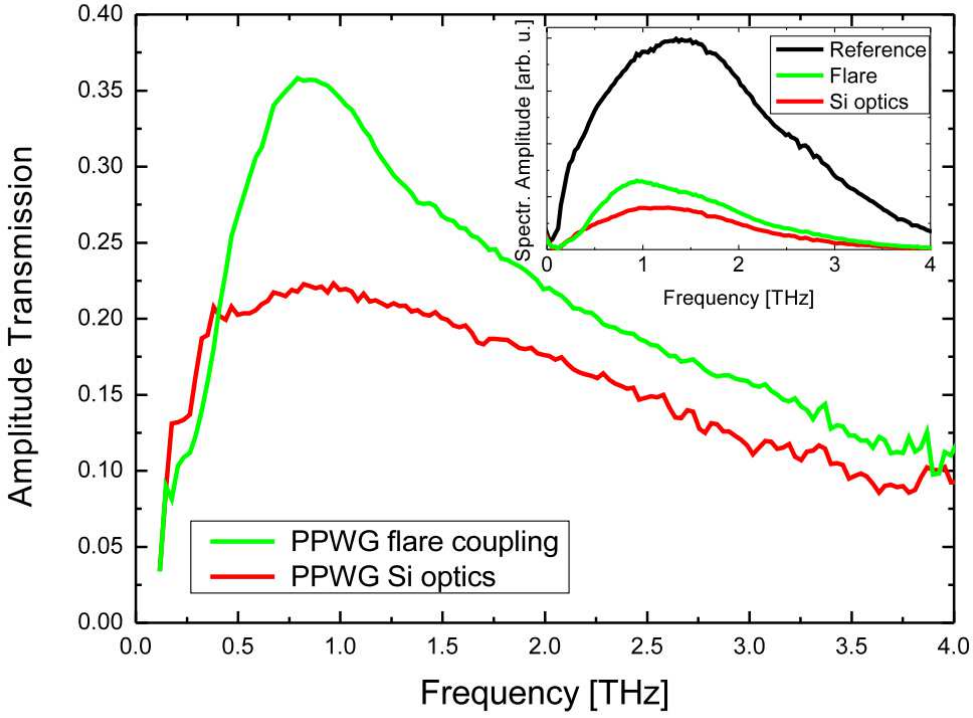

Figure 11: Frequency dependent transmission (coupling ratios) for the flare-coupled and silicon lens-coupled parallel-plate waveguides with a gap spacing of 50 μm. Inset: Spectral amplitude transmissions shown, including that for the reference pulse [19].

3.4.3 Solid metal tapers

The flexibility of the metallic shim flares had several advantages, given that it made the flares relatively easy to shape to whatever desired curvature and openings were needed to enhance either coupling or broadband capabilities. It was also easy to cut the flares to whatever length was needed, and different metals could be used based on their different conductivities. However, this very flexibility also presented several drawbacks. Being non-rigid, the shape of the flare was easy to disrupt merely by touch. Reproducibility of coupling through the flare-coupled waveguides was diminished, as continual use of the waveguides generated changes in flare shape, curvature, and opening widths. A more rigid and permanent coupling solution was needed.

I noticed that we had several aluminum cylinders in the lab, and that a chord cut from those cylinders exhibited a very similar flare-like shape, as shown in Figure 12. Adiabaticity could be controlled by the diameter of the cylinder chosen, and a PPWG could easy be incorporated onto the cylinder surface merely by flattening the middle. This cylindrical coupler could serve the same purpose as the flares by introducing an adiabatic compression into the parallel-plate waveguide. If the cylindrical coupler worked as desired, the resulting waveguides would be low-cost, easy to manufacture, and rigid. The cylindrical coupler could simultaneously remove the need for quasi-optic coupling and its associated losses while improving both coupling performance and reproducibility.

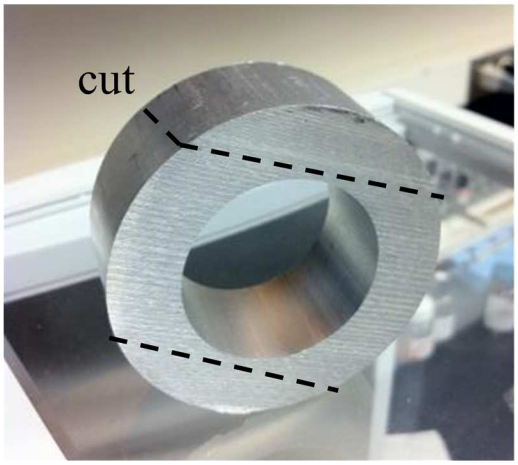

Figure 12: 2.5" diameter cylinder selected to be cut and used as a coupler; here, the positions of the cuts to create the chords are marked.

The coupler was crafted by machining away two chords of a desired thickness and depth from a hollow metal cylinder (in this case, aluminum). The dimensions of the 2 cylindrical chords are given in Figure 13. The chords were then inverted and coupled together; 4/40” screw holes were drilled into the chords – this method caused some issues, as screwing together two uneven surfaces presents challenges in aligning the chords to be parallel relative to one another, but for the most part, carefully adjusting the tightness of the screws as the pieces were bound together eliminated any problems with regards to changes in signal propagation through the chord structure. To finish off the fabrication, the surfaces of the chords were polished and smoothed before use.

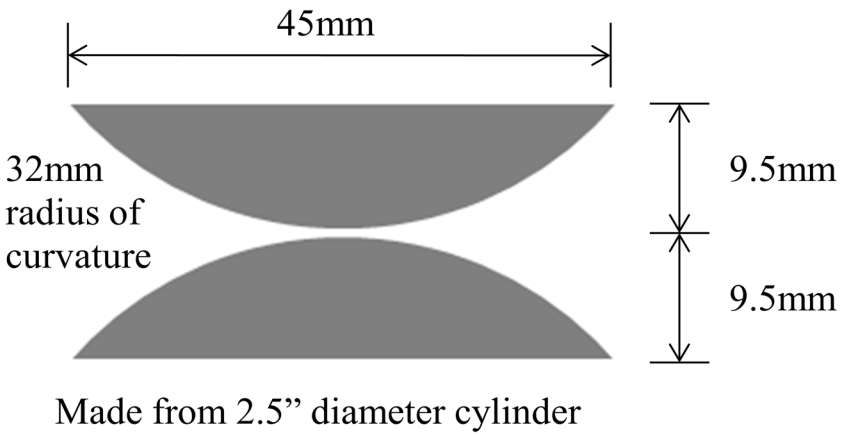

Figure 13: Dimensions of aluminum cylindrical chord. The width of the chord (not pictured) is ~ 25 mm, or 1 inch. The radius of curvature (ROC) of the chord cut from the 2.5 inch cylinder is 32 mm.

The cylindrical coupler was then placed directly into the beam waist of the THz-TDS system. To fully characterize the coupler, measurements were taken of the throughput of the THz signal with the coupler oriented in both TEM (TM_0) and TE modes. While TE propagation is not commonly used due to sharp cutoff frequencies, some interesting applications involving waveguide propagation in the TE orientation has been shown by others in the THz community [20]. With this in mind, I tested coupling performance in both polarizations. During testing, gap widths between the coupler plates were varied from 25 μm to 300 μm by placing brass spacers of known thicknesses just outside the beam extent on the inner surface of the couplers. Once in place, the plates were bolted together with screws and carefully adjusted so as to be as parallel as possible to one another. The coupler was then placed in the beamwaist at the center of the parabolic mirrors in the THz-TDS system, and oriented so as to operate in either TEM or TE propagation.

As with the silicon lenses and the flared waveguides, the couplers appeared to be dispersionless, demonstrated by Figure 14 [21]. In TM orientation, the coupler was found to have a coupling ratio of approximately 18% for gaps larger than 50 μm. This reduced to about 16% for gap sizes below 50 μm. At gap sizes of 100 and 150 μm, the higher-order TM2 mode can be seen.

Propagation of higher order modes is dependent upon the gap spacing between the waveguide plates, and for an air-filled waveguide is governed by the equation:

$$f_c = \frac{mc}{2d} \tag{11}$$

where m = mode number, c = speed of light, and d = gap size. The presence of higher order modes at gap sizes sufficiently large enough to allow their propagation is precisely why for most applications, the typical gap spacing for parallel plate waveguides is kept at around 50 μm. This helps to balance absorption losses with modal propagation. This holds true for the 2 cylinder coupler, even though the associated propagation length with the coupler is only 1 mm. Because of the small ROC, the actual gap separation varies somewhat quickly from the center of the waveguide, increasing by 2 μm for every 0.25 mm distance from the center. As a result, for a 25 μm gap with a propagation distance of 0.5 mm centered on the coupler axis, the actual plate (chord) separation varies from 25 to 27 μm. Correspondingly, the separation increases by 8 μm 0.5 mm from the center, or at a propagation distance of 1 mm centered on axis, which, for a desired gap of 100 μm gap, varies the actual gap width from 100 μm to 108 μm.. The coupling data in Figure 14 and Figure 15 clearly show that the higher order modes, entering at 150 μm at 2 THz and 100 μm at 3 THz, neatly follow the above equation. This result not only shows that our gap spacers are accurate, but shows the dispersionless nature of the coupling system. Note that Figure 15 demonstrates the frequency-dependent nature of the 2 cylinder coupler – as the frequency increases, so does the transmission. This is due to the smaller wavelength of the higher frequencies, which, being more focused at the center of the THz beam, improves in coupling as the intensity is centered more closely to the symmetry axis.

As shown in Figure 16, rotation of the coupler by 90º to operate in TE propagation shows lower dispersion and significantly sharper cutoff frequencies than for the silicon-coupled PPWG counterpart seen in Figure 17 [21]. The demonstrated cutoff frequencies are very near the

theoretical cutoff frequencies described by Equation (11). The lower dispersion is due, in part, to the much smaller propagation distance of 1 mm for the 2 cylinder coupler. Oscillations for the silicon-coupled waveguide continue well on past 100 ps (not shown in Figure 17), but for the 2 cylinder coupler occur for less than 50 ps. The frequency cutoff is also significantly sharper (22x more so) for the first order TE1 mode than for the silicon-coupled waveguide (although for the latter, some loss is attributable to absorption on the surface of the parallel plates). This demonstrates that the adiabatic coupler improves the amplitude transmission above the given cutoff frequencies and also eliminates the troublesome reflection from the silicon lenses.

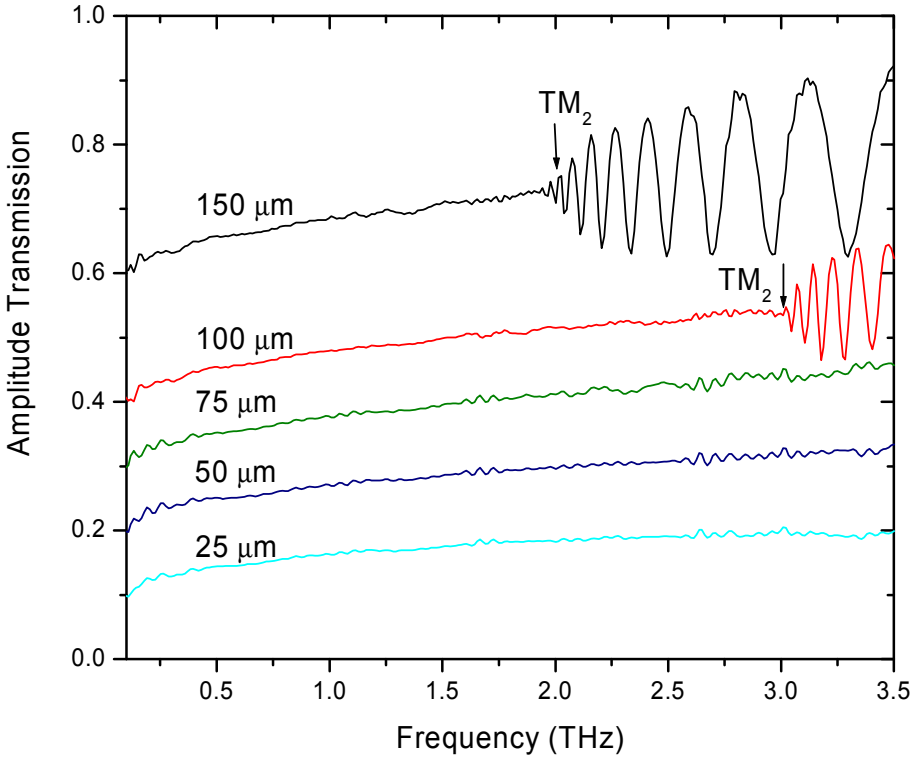

Figure 14: Transmission of the THz wave through the 2-cylinder 32 mm ROC coupler in TEM (TM_0) propagation with varying gap spacing. For visual clarity, the data presented has been separated by 0.1 between the 25, 50, 75, and 100 μm gaps and by 0.2 between 100 and 150 μm gaps [21].

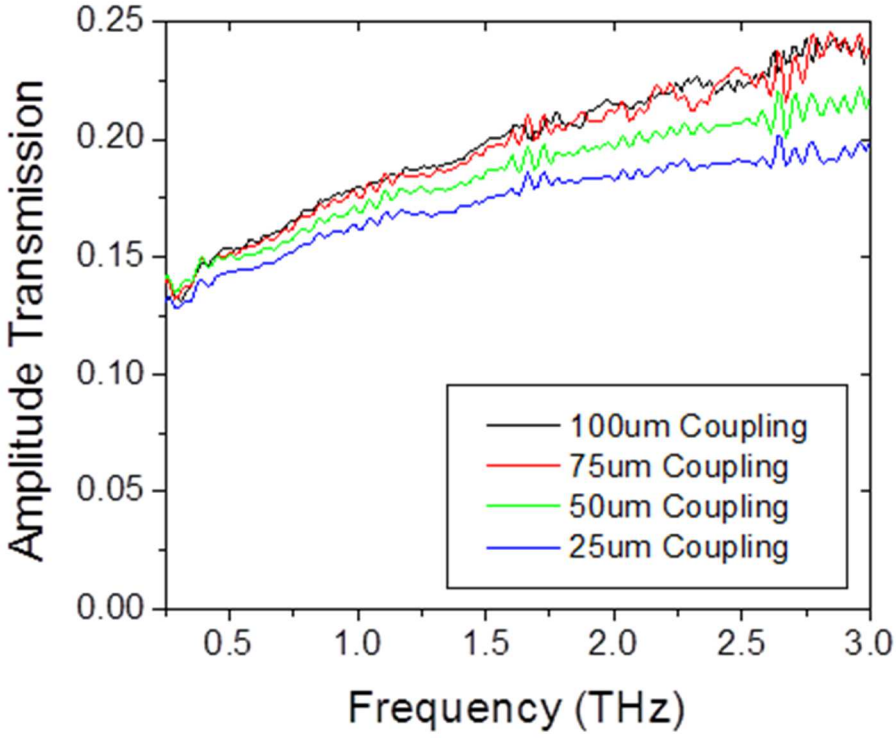

Figure 15: Frequency dependent transmission of the 2 cylinder coupler.

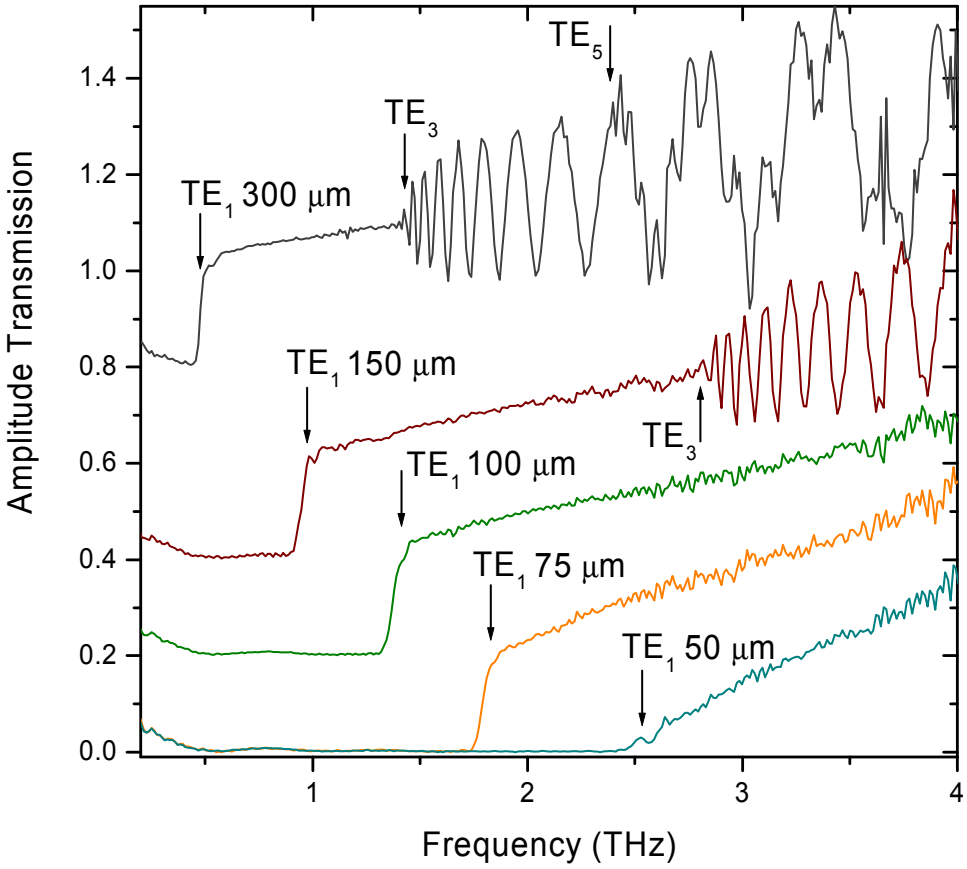

Figure 16: Transmission of the THz wave through the 2-cylinder 32mm ROC coupler in TE orientation with varied gap spacing from 50 μm to 300 μm. For visual clarity, the transmission lines have been separated by 0.2 between the 75, 100, and 150 μm gaps and by 0.4 between 150 and 300 μm gap [21].

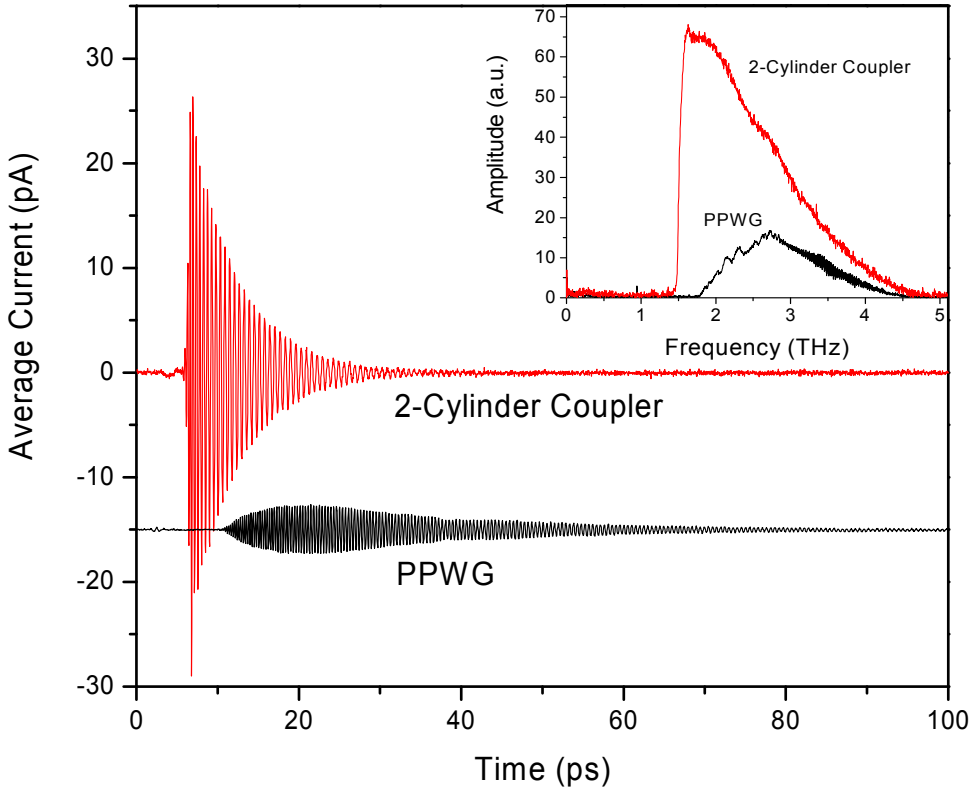

Figure 17: Comparison of THz pulse propagation through the 32 mm ROC 2-cylinder coupler and a silicon lens coupled PPWG with 100 μm gap in TE_1 mode propagation. INSET: Comparison of the transmission through the cylindrical coupler and a PPWG [21].

4. CYLINDRICALLY-COUPLED PARALLEL-PLATE WAVEGUIDES

This section builds on the previous results and describes the integration of a solid metal cylindrical coupler with our standard metal THz parallel plate waveguides (dimensions of the standard PPWG are described in Section 3.1). Research and evidence had made it clear that the more adiabatic the waveguide, the better the coupling would be. With this in mind, two iterations of the cylindrically-coupled parallel-plate waveguide (CYLWG) were created: 1) using a 4-inch radius of curvature cylinder (4 ROC CYLWG), and 2) using an 8-inch radius of curvature (8 ROC CYLWG).

4.1 Background

The term "adiabatic" has many meanings. It has evolved from quantum theory and thermodynamics and is loosely defined as "slowly varying" [22 – 25]. In essence, it refers to a system whereby the parameters are varied in such a way as to allow the system to remain in its original eigenstate. This can also apply to guided wave theory. A guided wave can be adiabatically transformed from one method of propagation to another, if done in such a way as to not introduce reflections or convergence into higher-order modes [26 – 35]. This has, in fact, been applied to patented work as early as 1948 [36] and even in some previous work in the terahertz regime [11] [37].

A waveguide taper is used in microwaves to match devices with different cross-sectional areas and/or mismatched impedances by introducing adiabaticity across the boundaries (a horn antenna is an example). There are many kinds, but they all rely on the principle of using a taper (linear,

sinusoidal, exponential E-plane, H-plane, pyramidal, to name a few) across a length to match the impedances at either end of the structure. A circular waveguide taper, similar to one we are using for the CYLWG, works best when the radius is related to distance along the taper by a function that is smooth and has a zero first derivative at both ends. This means that the taper perfectly matches the change in waveguide dimensions at either side, since a non-zero first derivative would indicate a change in curvature, causing reflections [38]. As long as the as the taper is introduced over a length of many wavelengths, the reflections are negligible [31].

For our initial taper, the 32 mm radius of curvature, 2-cylinder taper seen in Figure 13, the length of the taper is 22.5 mm on either side. Compared to the 300 μm wavelength of 1 THz – the taper is 75x longer, sufficient to meet the adiabaticity criteria.

The 4ROC CYLWG and 8 ROC CYLWG tapers are both longer than 22.5 mm; therefore, the CYLWGs meet adiabaticity criteria for reflectionless (or near reflectionless) transmission. For the most part, all losses are due to conduction loss, a function of plate separation, which is examined more thoroughly in Section 4.4 Gap independent conduction loss.

4.2 Machining the cylindrically-coupled waveguides

For the 4 ROC CYLWG, as with the chords from the previous section, two new chords were cut from an aluminum cylinder using a larger radius of curvature (see Figure 18). The center of each chord was smoothed to a flat surface of 1 cm in length, requiring only a minimal amount of material to be removed. This small amount of flat plate was not standard to the dimensions of the parallel plate waveguides, but given the sharper curvature of the 4-inch radius plates (when compared to the 8-inch), this smaller flat region helped to ensure that the transition between coupler and parallel plates would not be sharp enough to perturb the incoming THz pulse, yet still provide enough surface space for spectroscopic samples to be deposited if desired. As before, the

waveguide was placed into the beamwaist of the THz system and the transmission through the waveguide was recorded for various gap spacings.

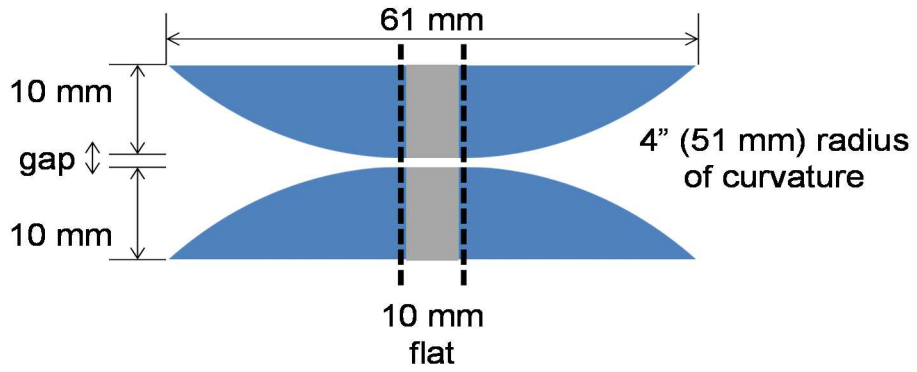

Figure 18: Top-down view of the dimensions for the 4 ROC CYLWG. Not shown is width of waveguide, which was 1", or about 25.4 mm.

As with the coupler, 4/40" screw holes were drilled into the pieces, placing countersunk through holes on one plate and tapped holes on the other. These screw holes were placed 0.59" (15 mm) apart from the vertical axis of the plates, causing them to be just outside the flat edge on the cylinder, and 0.413" (10.5 mm) outside the beam extent from the horizontal axis of the plate. The curved cylindrical surface was smoothed and finished before the parallel-plate section was cut to ensure that the coupling section did not introduce any unintended perturbations.

A second integrated waveguide was produced using a larger 8-inch radius of curvature, incorporating a 3 cm flat into the center of the curve to match that of our standard PPWGs. As shown in Figure 19, the 8 ROC CYLWG has a milled 28x30 mm parallel plate region that matches the PPWG seen in Figure 6. (This increase in flat plate length removed significantly more material than was required to create the 1 cm flat on the 4-inch ROC CYLWG, raising concerns about a potential transition mismatch between the coupling section and the parallel plates. Fortunately, in testing the device, no additional reflections, and therefore, no mismatch, were found in the data.) We also used two different kinds of metal, creating both aluminum- and

copper-pairs of waveguides. The different materials allowed us to measure the frequency dependent conductivity (see 3.2 Theory of operation).

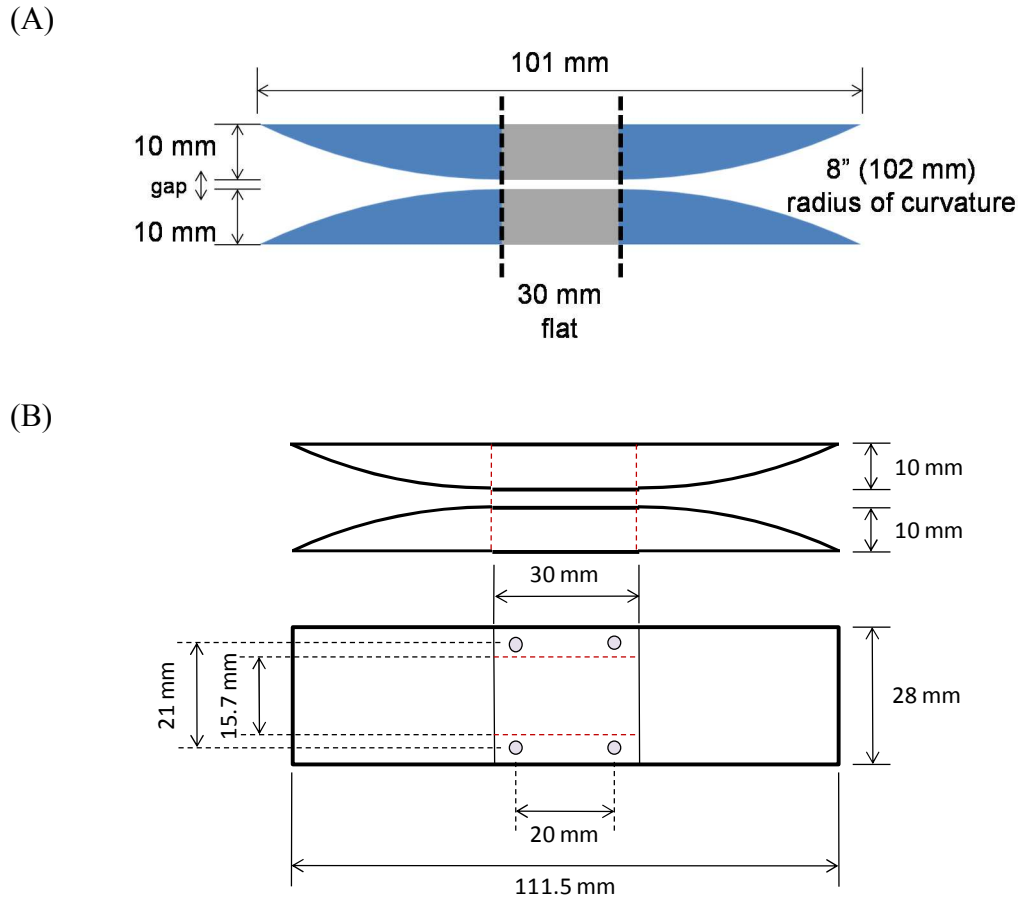

Figure 19: Dimensions of the 8 ROC CYLWG. (A) Top down view showing clearly (color version) the flat portion of the waveguide versus the cylindrical couplers. (B) Diagrams the plate of the waveguide showing the milled out 28x30 mm parallel plate region. The dotted red lines (color version) near the edges of the flat section indicate placement of the waveguide spacers [12].

For this larger waveguide, the 4/40" screw hole section was again drilled to match the previous layout, which in turn matched the original layout for the silicon lens-coupled PPWGs. The curved surface of the waveguide was smoothed and finished before milling the flat parallel-plate region. The dotted red lines (color version) near the edges of the flat region in (B) indicate placement of the waveguide spacers, which fit precisely into that region with punched holes to allow passage of

the connection screws. Between the dashed red lines is the open 15.7x30 mm area of the waveguide.

4.3 Performance of the CYLWG

To test the performance of both waveguides, spacers were cut using metal shims of known thickness and placed on the parallel-plates of each waveguide, outside the beam extent near the screw holes for each guide. The thicknesses of the spacers were varied from around 12.5 μm to 100 μm. With the addition of the parallel-plate section to create a flat working surface, this time assembling the waveguides was easy. Once the spacers were in place, the 4/40" screws needed to be placed into the screw holes and tightened between the guides. The fully assembled waveguide was then placed on axis in the beamwaist of the THz-TDS system. To compare the waveguides, reference pulses were measured and then the waveguides were assembled with equal spacing and subsequently measured with equivalent air-gaps. To measure the conductivities of the waveguides, several pulses were measured and averaged together for various gap spacings. The data was zero-padded to help ensure smoothness of the final data sets.

Notes on zero padding:

Zero padding is often used in THz-TDS. Extending the time domain pulse data with zeros causes the subsequent Fourier transform to perform an interpolation in the frequency domain between the linearly independent real data points, separated from each other by 6.67 GHz for a 150 ps scan length. This interpolation occurs between the existing data points and, because the pulse has already dampened into the noise floor, does not increase the frequency resolution of the measurement. This is most commonly helpful when examining low-absorption spectral transmission as it does not shift the spectral frequencies of the absorption lines nor does it affect the line shape. It is also so commonly used

because avoidance of pulse reflections, most notably caused by the silicon lenses used to couple to the waveguides, caused early truncation of the THz pulse and subsequently, resulted in a broadened line shape accompanied by small spectral shifts in the frequency domain. Zero padding helps to make the points of spectral absorption more clear.

For the first comparisons, both waveguides were assembled using a gap spacing of 50 μm and left empty (air-filled). A reference pulse through the THz-TDS system was recorded. Then each waveguide was placed on axis into the system beamwaist and the corresponding pulses were measured. To compare their coupling performances, ratios were taken with respect to the reference pulse.

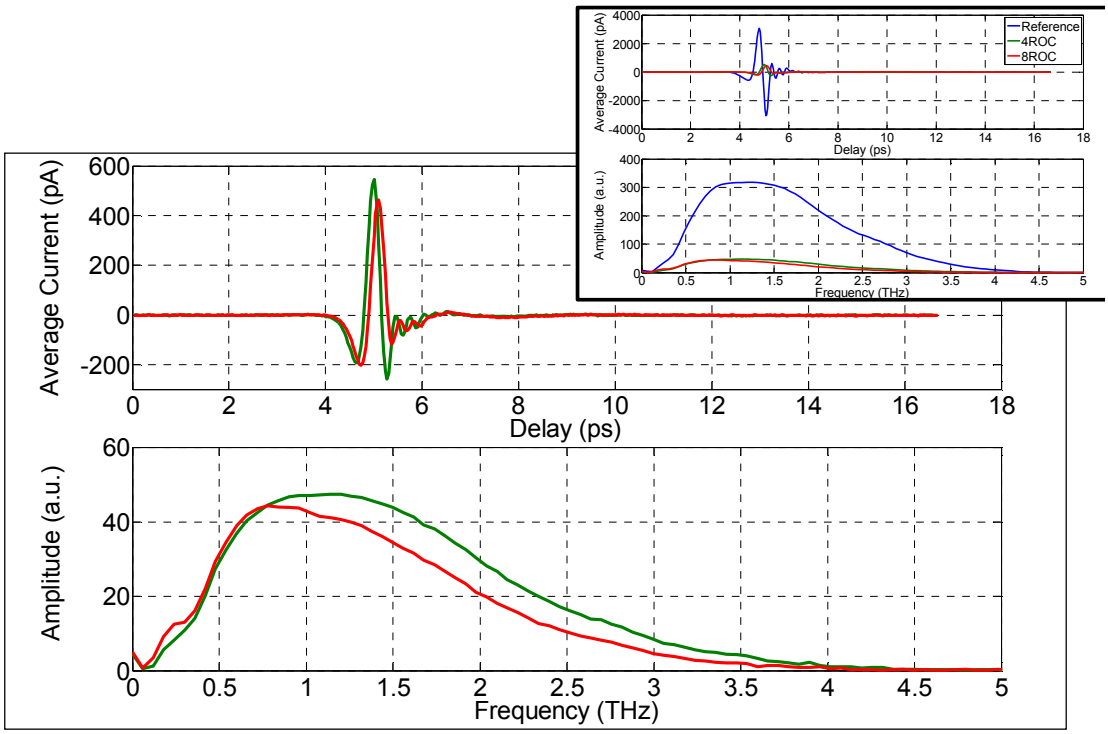

Figure 20: Pulses through the air-filled 4ROC and 8ROC CYLWGs (top) and their corresponding spectra (bottom). Inset: The reference pulse is included (blue line) for comparison.

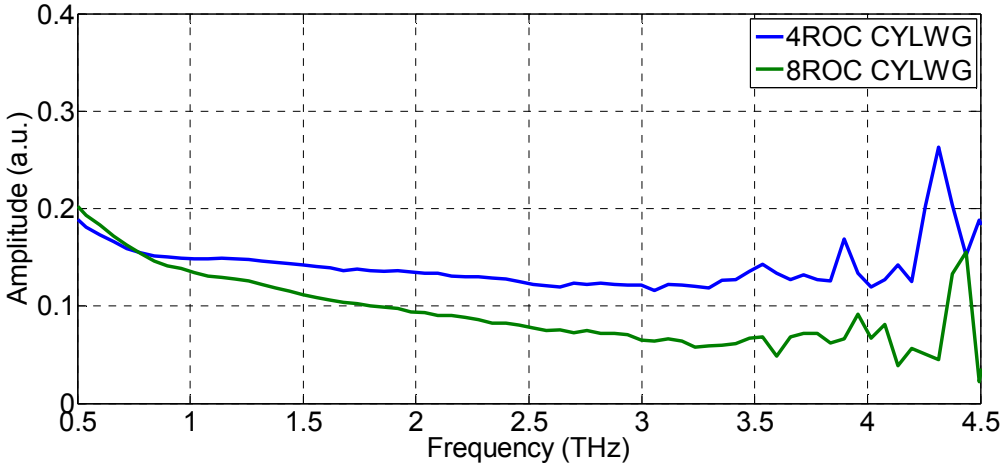

Figure 21: Coupling comparison between the air-filled aluminum 4 ROC CYLWG and aluminum 8 ROC CYLWG with equal gap spacing of 50 μm.

Surprisingly, as shown in Figure 20 and Figure 21, the more adiabatic 8 ROC waveguide did not show an enhanced coupling performance over the more quickly-varying cylindrical coupler. Overall performance for both waveguides was similar, although the coupling for the 8ROC CYLWG shows a much stronger frequency dependent loss due to the stronger conductive losses presented by the longer interaction length of the 3 cm integrated parallel-plate. When the coupling ratios were modified to examine the absorbance spectrum of each waveguide, the 4ROC waveguide exhibited broadband absorption for each gap size. As seen in Figure 22, for 50, 75, 100 μm gap sizes, the transmission through the 4ROC CYLWG is nearly frequency-independent (the higher absorption seen at 25 μm is most likely due to imperfections in the surface of the waveguide, as well as the shims used to create the gap spacers, causing extreme variations at a smaller gap). The overall transmission, however, is slightly lower than predicted by the 2-cylinder, 32ROC coupler discussed in Section 3.4.3 Solid metal tapers. This is most likely due to the increased conduction losses presented by the addition of the integrated 10 mm parallel-plate section.

The 8ROC waveguide exhibited something much more interesting, displaying a frequency-dependent coupling similar to the flared waveguides (see previous section). This led to further investigations on coupling performance for the 8ROC waveguide to determine the nature of these conduction losses on the absorption of the waveguide.

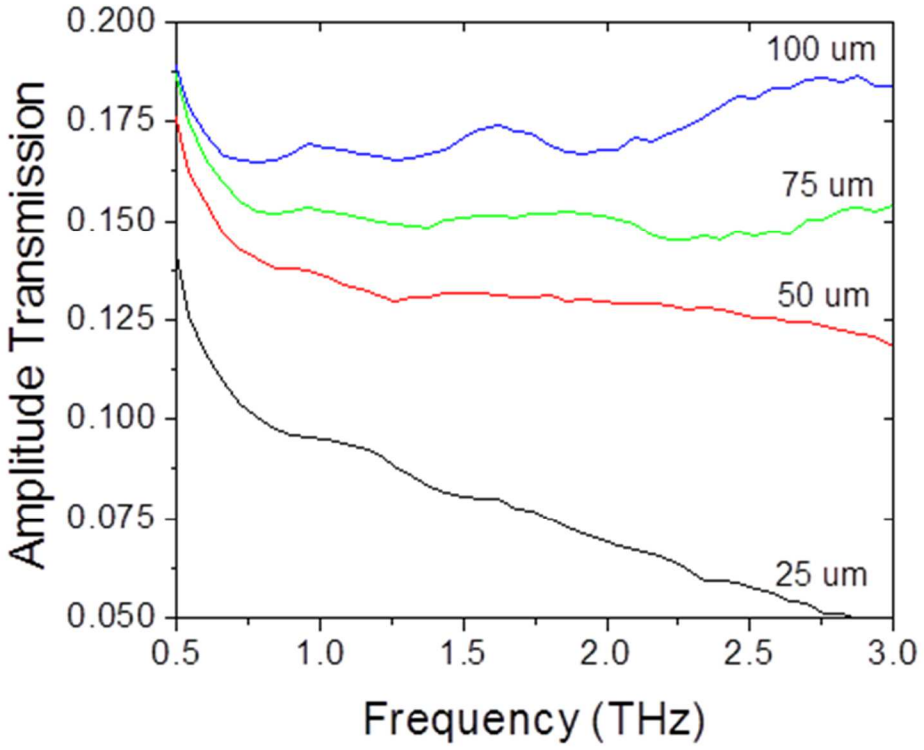

Figure 22: Transmission for the 4ROC CYLWG with several gap spacings.

4.4 Gap independent conduction loss

In 2007 this lab became interested in trying to enhance spectroscopic signatures by improving the conductivity of the metal waveguides the samples were deposited on. It was initially thought that by cooling the waveguides to liquid nitrogen temperatures (77 K), temperature dependent phonon interactions would be reduced, enhancing the conductivity of the metals at cooler temperatures (as seen in Figure 23). Instead, it was found that lattice defects play a much larger, dominant role in determining carrier scattering [39].

This previous work suggested that the relatively large waveguide absorption losses were largely dependent upon the reduced conductivity of the skin depth layer which occurred because of these surface and lattice defects. Because the nature of the silicon lenses used with the quasi-optical PPWGs only allowed a fixed and limited amount of THz signal compression into the sub-wavelength confinement of the guide, measuring the conductivity of the parallel plates was challenging, as the coupling did not remain constant when the plate separation was changed. Since absorption, and consequently, conductivity measurements are based on the waveguide assembly's ability to couple in radiation, inconsistent coupling can produce erroneous results. With the introduction of the 8ROC CYLWG, constant coupling of the THz wave, independent of gap size between the parallel plates, can be demonstrated. Fresnel losses and reflections are removed; the gap independent conductivity can now be measured.

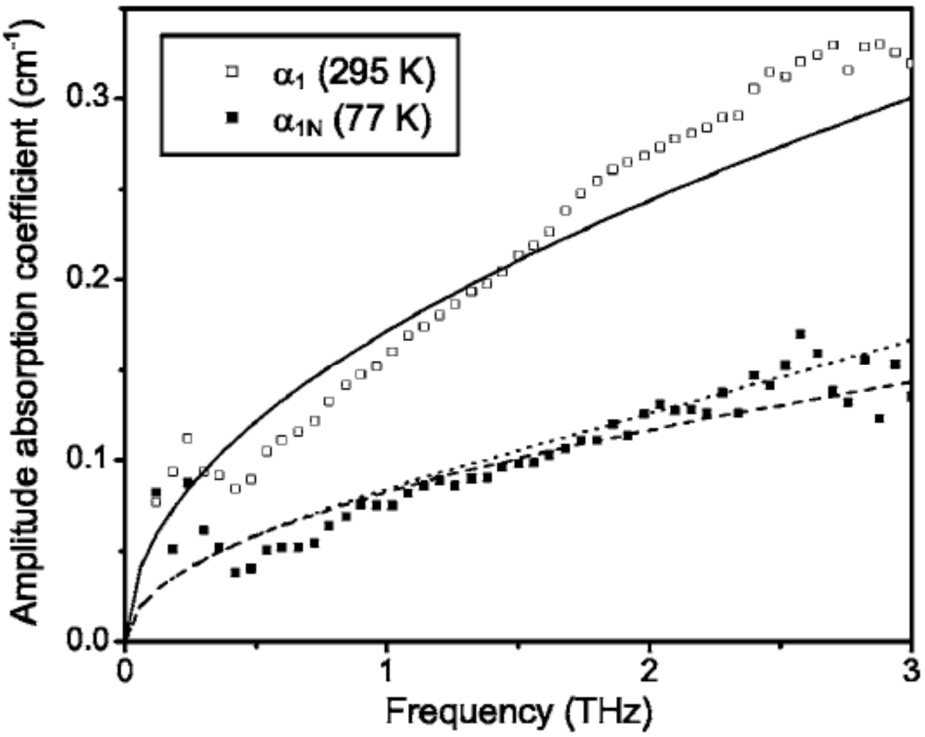

Figure 23: Waveguide amplitude absorption coefficient for a silicon-lens coupled PPWG [39]. The hollow squares are the data measured at 295 K (room temp) and the solid squares at 77 K (liquid nitrogen). The solid lines are the theoretically predicted data [39].

The transmission measurements through the aluminum 8ROC CYLWG waveguide showed that the CYLWGs performed as well as the silicon-lens coupled PPWGs. Figure 24 shows the transmitted pulses (top) and the spectral data (bottom) for free-space and the waveguide with different plate spacings. Figure 25 shows the transmission measurements through the aluminum 8ROC CYLWG without the reference pulse, as does Figure 26 for the copper 8ROC CYLWG.

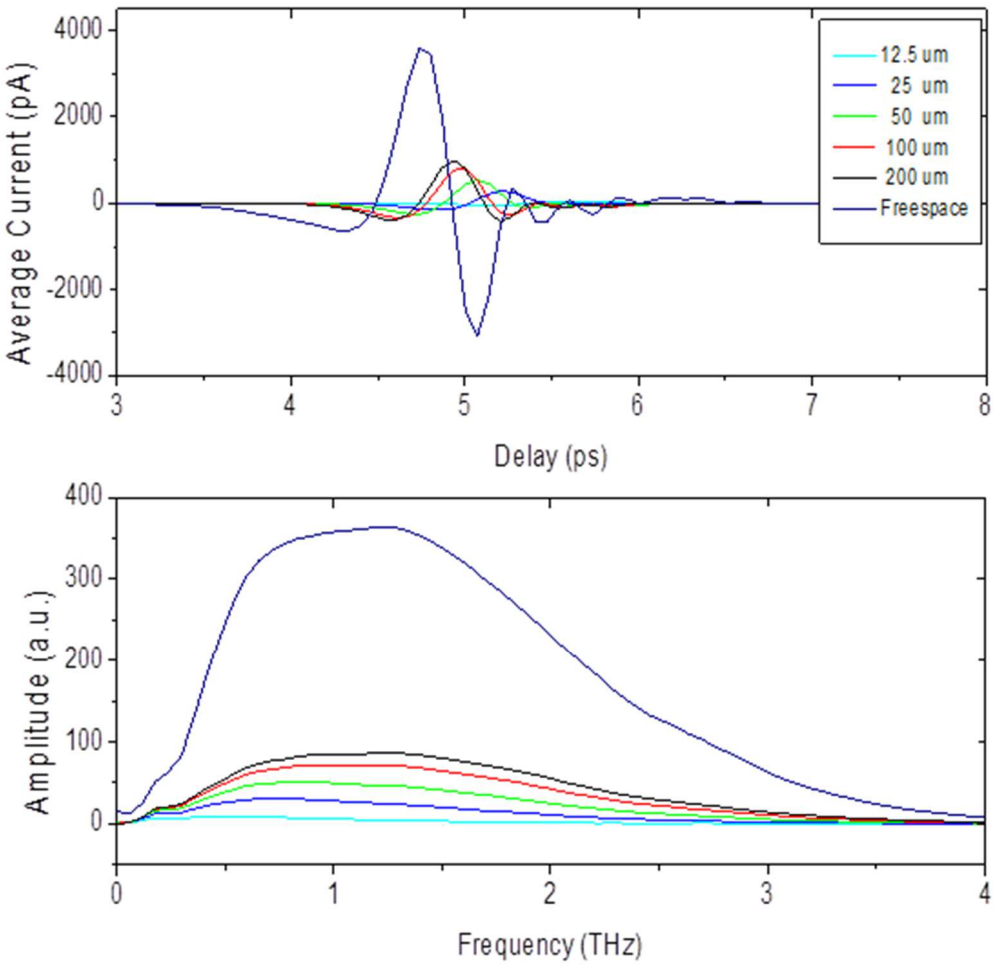

Figure 24: (Top) Transmitted THz pulses through the air-filled aluminum 8ROC CYLWG with various gap spacings and the corresponding system reference pulse through free space. The measured pulse durations have been cut to show only from 3 to 8 ps for clarity. (Bottom) Corresponding amplitude spectra for each pulse [12].

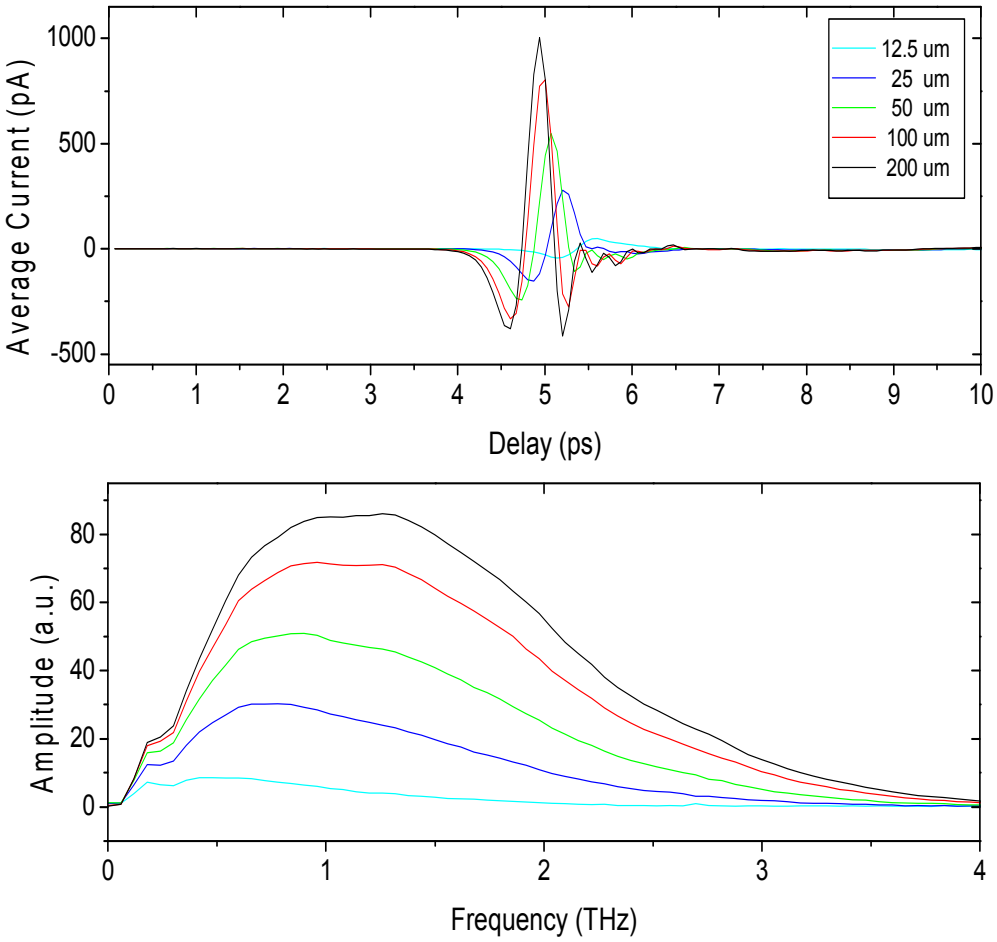

Figure 25: This figure shows the same data from the previous figure without the associated system reference pulse. (Top) Transmitted THz pulses through the aluminum 8ROC CYLWG. (Bottom) Corresponding amplitude spectra for the pulses [12].

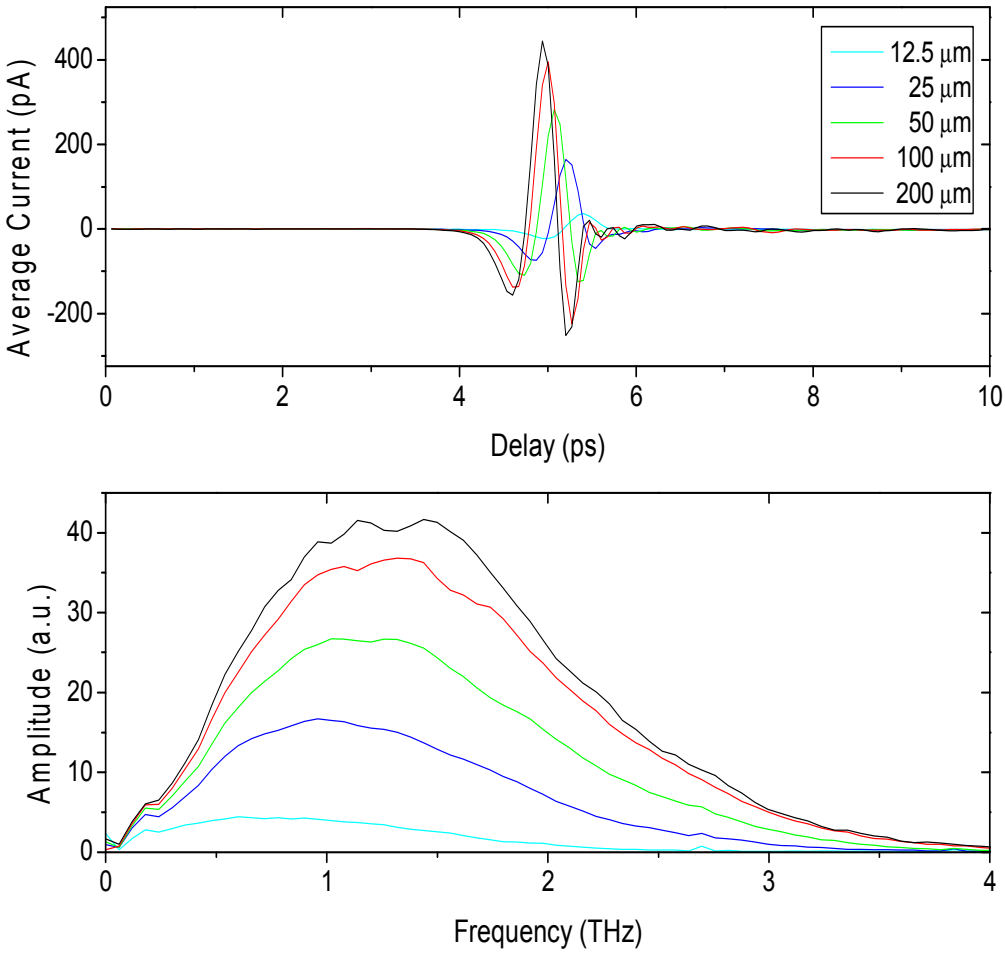

Figure 26: This figure shows pulses through an 8ROC CYLWG manufactured from copper. Reference pulse not given. (Top) Transmitted THz pulses with various gap spacings. (Bottom) Corresponding amplitude spectrums [12].

In Figures 24-26, the decrease in transmission with smaller gaps is clearly seen. As shown in Figure 24 for a 200 µm gap, the transmission through the waveguide at 1 THz is 22 %. However, removal of absorption effects shows the coupling to be 28%, comparable to that of silicon lenses [14]. The following analysis [12] will show that this coupling is constant for all gap sizes, and that the reduced transmission occurs due to absorption in the skin-depth layer of the metal.

The reflectionless transmission of THz pulses through the CYLWG is initially assumed to be a function of the gap size and the absorption at each gap designated by g, as given below, which follows the analysis of Reference [12]:

$$T_g = C_g(\omega)e^{-\alpha_g(\omega)L} \tag{12}$$

where T_g is the amplitude transmission, C_g is the (initially assumed gap dependent) frequency dependent coupling into and out of the TEM mode of the CYLWG, α_g is the TEM-mode, gap-dependent absorption, and L is the 30 mm length of the flat parallel-plate region of the CYLWG. The amplitude spectrum $A_{t,g}(\omega)$ transmitted through the waveguide is given by the free-space input pulse spectrum, $A_o(\omega)$, multiplied by the CYLWG transmission T_g:

$$A_{t,g}(\omega) = A_o(\omega)T_g = A_o(\omega)C_g(\omega)e^{-\alpha_g(\omega)L} \tag{13}$$

$A_{t,g}$ can be seen in Figs. 24-26. The comparison with free-space transmission for the aluminum CYLWG is also shown in Figure 24. To show that the waveguide coupling is independent of gap and that the changes in transmission with gap are only due to absorption effects, we first examine the relative coupling of the waveguide with respect to the largest gap size of 200 μm, rather than to free-space. This ratio will demonstrate that the amplitude coupling Cg is independent of gap. These relative transmission measurements are given by:

$$\frac{A_{t,g}(\omega)}{A_{t,200}(\omega)} = \frac{C_g(\omega)}{C_{200}(\omega)}e^{-(\alpha_g-\alpha_{200})L} \tag{14}$$

The relative absorbance RA = $(\alpha_g - \alpha_{200})L$ for each gap is obtained from Eq. (3) as:

$$RA = (\alpha_g - \alpha_{200})L = \ln\frac{C_g(\omega)}{C_{200}(\omega)} - \ln\frac{A_{t,g}(\omega)}{A_{t,200}(\omega)} \tag{15}$$

Dividing RA by the 3 cm length of the parallel-plate region gives the relative absorption coefficient of the waveguide, shown in Figure 25 as the lower dash-dot-dot lines for the aluminum CYLWG, and also in Figure 26 for the copper CYLWG.

As already discussed in Section 3.2 Theory of operation, the theoretical absorption coefficient for the parallel plate metal waveguide is well known and is given in textbooks and handbooks [13] [40]:

$$\alpha_0 = R/(\eta_0 b)\ (m)\text{-}1 \tag{16}$$

$$R = 10.88 \times 10^{-3}[10^7/(\sigma\lambda_0)]^{0.5}\ \Omega \tag{17}$$

where R is the metal impedance, η_0 is the free-space wave impedance of 377 Ω, b is the gap size, and σ is the conductivity of the metal.

The dependence on frequency and conductivity becomes clear when the two equations are combined to form the simpler mathematical expression in Eq. (7), where the frequency f is expressed in units of THz, or 10^{12}, σ is in terms of 10^7 (Ω·m)-1, and η_0 is replaced by 377 Ω.

$$\alpha_0 = 1.6662 \times 10^{-3}\left[\frac{f}{\sigma}\right]^{0.5}\left(\frac{1}{b}\right) \tag{18}$$

From this equation, it is now explicitly apparent that the absorption has both a $\sqrt{f}$ dependence and an inverse proportionality to b. We can use this simple dependence to test the accuracy of our observations, given in Figure 25 and Figure 26, and to show that we have coupling independent of gap size. The results of our observations, shown in Figure 27 and Figure 28, exhibit a good $\sqrt{f}$ dependence fit (dashed lines) and the absorption is almost inversely proportional to b, confirming that $\ln\frac{C_g(\omega)}{C_{200}(\omega)} = 0$, and equivalently $\frac{C_g(\omega)}{C_{200}(\omega)} = 1$. Eq. (3) can now be rewritten with $C_g(\omega)$ simplified to $C(\omega)$:

$$\frac{A_{t,g}(\omega)}{A_{t,zero\ \alpha}(\omega)} = \frac{C(\omega)}{C(\omega)}e^{-\alpha_g(\omega)L} \tag{19}$$

The measurements can now be normalized to the no-absorption waveguide by noting that the b dependence shows $\alpha_{100} = 2\ \alpha_{200}$:

$$\frac{A_{t,100}(\omega)}{A_{t,200}(\omega)} = e^{-(\alpha_{100}-\alpha_{200})L} = e^{-(\alpha_{200})L} \quad (20)$$

Consequently, the 200 µm absorbance can be added to all the curves to obtain the actual absorption coefficients, as given by the solid lines in Figure 27 and Figure 28, marking the top of the highlighted regions indicating the addition.

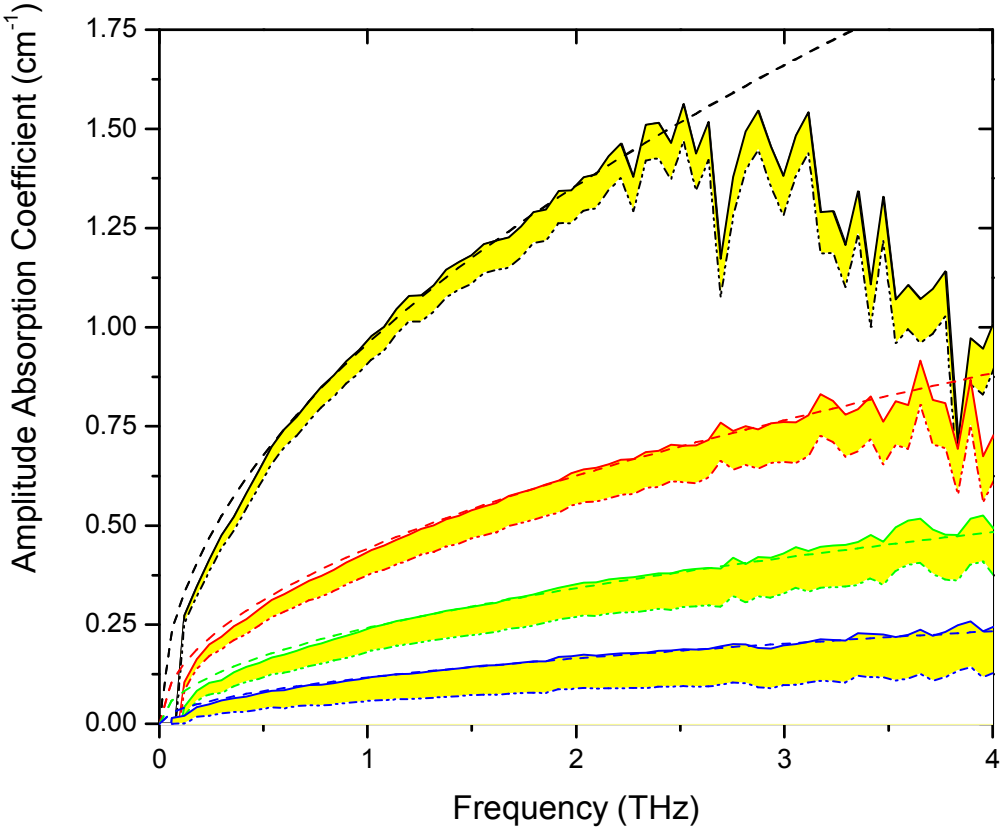

Figure 27: Absorption for an aluminum 8 ROC CYLWG. From top curve gap, g=11.9 µm, g= 22.5 µm, g = 50 µm and bottom curve g=100 µm [12].

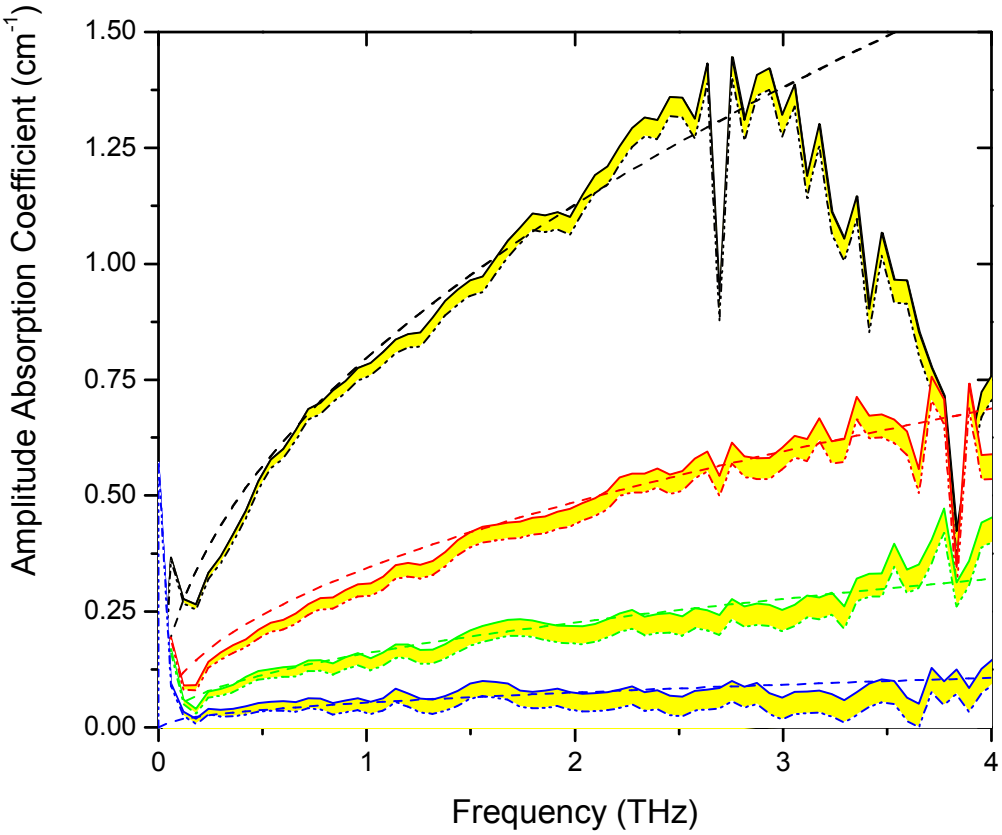

Figure 28: Absorption for a copper 8 ROC CYLWG. From top, g=10 μm, g=23.4 μm, g=50 μm, and bottom curve g=100 μm [12].

Table I. Measured strength parameters S of the different gaps, given in units of 1/cm. To obtain the absorption coefficient, multiply by $\sqrt{\mathbf{f}}$ in THz. Note that S = α at 1 THz [12].

Aluminum	**11.9μm**	**22.5μm**	**50μm**	**100μm**
S	0.95	0.445	0.25	0.120

Copper	**10μm**	**23.4μm**	**50μm**	**100μm**
S	0.78	0.33	0.155	0.054

As stated previously, the measurements shown in Figure 27 and Figure 28 exhibit a good fit to the $\sqrt{f}$ dependence (dashed lines). These calculated $\sqrt{f}$ fits have been multiplied by the strength parameter S, given in Table I, adjusted to achieve the best fit to the total measured absorption, for which the 200 μm absorption has been added to the relative absorption (dash-dot-dot) lines. These accurate fits verify that our waveguides have constant coupling over the range of gap sizes, in contrast to the gap dependent overlap integral description of the quasi-optical coupling of the silicon lenses to the PPWG [8] [3].

As given in [12], as the 8ROC CYLWG's gap becomes smaller and smaller, it continues to provide adiabatic compression for radiation, limited only by the flatness of the plates (for perfect conductors). For air-space normal metal plates, the minimum gap is determined by the general condition that the absorption coefficient α_{gLimit} due to waveguide loss must be less than $1/\lambda$, where λ is the guided wavelength [41]. When α_{gLimit} approaches this limit, the approximations made in obtaining the wave equation solutions for the transverse waveguide modes breaks down and the lumped element regime of electronics is approached. For our CYLWG situation, if we set $\alpha_o = \alpha_{gLimit} = 1/\lambda o$, and solve for b at the frequencies 0.5 (600 μm), 1.0 (300 μm) and 2 (150 μm) THz, we obtain the gaps b of 0.37 μm, 0.26 μm and 0.18 μm, respectively. It is reasonable to assume that an absorption length (1/e for amplitude) of 10 wavelengths would still give good waveguide propagation, which corresponds to the limiting operational gaps b of 3.7 μm, 2.6 μm and 1.8 μm, for 0.5, 1 and 2 THz, respectively. These results are important to understand the fundamental sensitivity limits of waveguide THz-TDS.

The inverse proportionality to gap size is also evident, as shown in Table 1, for which the absorption coefficient for each gap is given by the strength parameter S, in units of 1/cm, multiplied by $\sqrt{f}$, where f is the frequency in THz. Here, the measured thicknesses of the metal

spacers used to create the gaps are given. The deviations from a strict 1/b dependence is considered to be due to not having flat surfaces over the waveguide plates, for which smoothly varying surface features of the order of microns were present.

As shown here and in [12], by substituting into Eq. (7) the measured absorption value, the specified frequency, and the gap size, the conductivity factors of the waveguide metals were determined. For aluminum, the measured conductivity factor was 1.9, and for copper, 3.5 was obtained. The handbook conductivity factors for aluminum and copper are 3.72 and 5.80, respectively [40]. For each metal, the measured conductivity in the THz skin depth layer is significantly less than the bulk value. As seen in previous publications [39], this reduction in conductivity is expected and can be attributed to carrier scattering due to lattice defects in the surface layer.

Table 2: Comparison of measured absorption and conductivity values to theoretical (book) values. Note that the given absorption values are measured at a 25 μm gap spacing.

ABSORPTION $(cm)^{-1}$	**Aluminum**	**Copper**
Measured	0.47	0.5
Theoretical	0.50	0.39
CONDUCTIVITY $(\Omega cm)^{-1}$		
Measured	1.9×10^7	3.5×10^7
Theoretical	3.54×10^7	5.8×10^7

The loss free coupling of 28% of the reflection-free 8ROC CYLWG is comparable to the silicon-lens based method of coupling with 32% for the best case [42]. The major advantage is that the frequency dependent coupling of the easily assembled 8ROC CYLWG is quite reproducible and is independent of the waveguide gap. Given flat, smooth surfaces on the waveguide plates, the

gaps could be reduced to 5 μm and still retain the same coupling, which would be impossible to do with the gap dependent coupling of the silicon-lens coupled waveguides. The reflection free CYLWG waveguides are also significantly easier to use, since there are no additional lenses or other parts that need to be precisely aligned.

4.5 Application: Using the CYLWG in spectroscopy

To satisfy our interest in proving that removing the silicon lenses would allow us to extend our scan length, and by way of that, possibly increase our spectroscopic sensitivity, we performed an example measurement of a spectroscopic sample of lactose dropcast onto the smooth (flat) portion of 4ROC CYLWG, and compared the measurements with a previous set done on the standard quasi-optical parallel-plate waveguide. Lactose was chosen simply because it has a few well-known, very strong, resonant features within the THz bandwidth. For our purposes, we focused primarily on the two resonances located at 0.53 THz and at 1.4 THz. The 0.53 THz resonance is one of the narrowest known lactose; the 1.4 THz resonant line is the strongest.

In previous measurements, our lab was able to resolve the 0.53 THz resonant line to around 6.3 GHz using the quasi-optical method of coupling with a PPWG (see Figure 31). It was our hope that if there was more spectral information included in the tail of the waveform, the 4ROC CYLWG would now be able to read that information and, hopefully, resolve the resonant lines even more sharply by scanning out over a longer delay without reflection interference.

Measurements were initially made on the 4ROC CYLWG at room temperature. Once we verified that we could see the sample, we then placed the waveguide into the cryogenic cooler, chilling the waveguide sample to 10K where the final, high resolution measurement was made. The result was then plotted for comparison to a lactose sample similarly measured on a silicon-lens coupled PPWG.

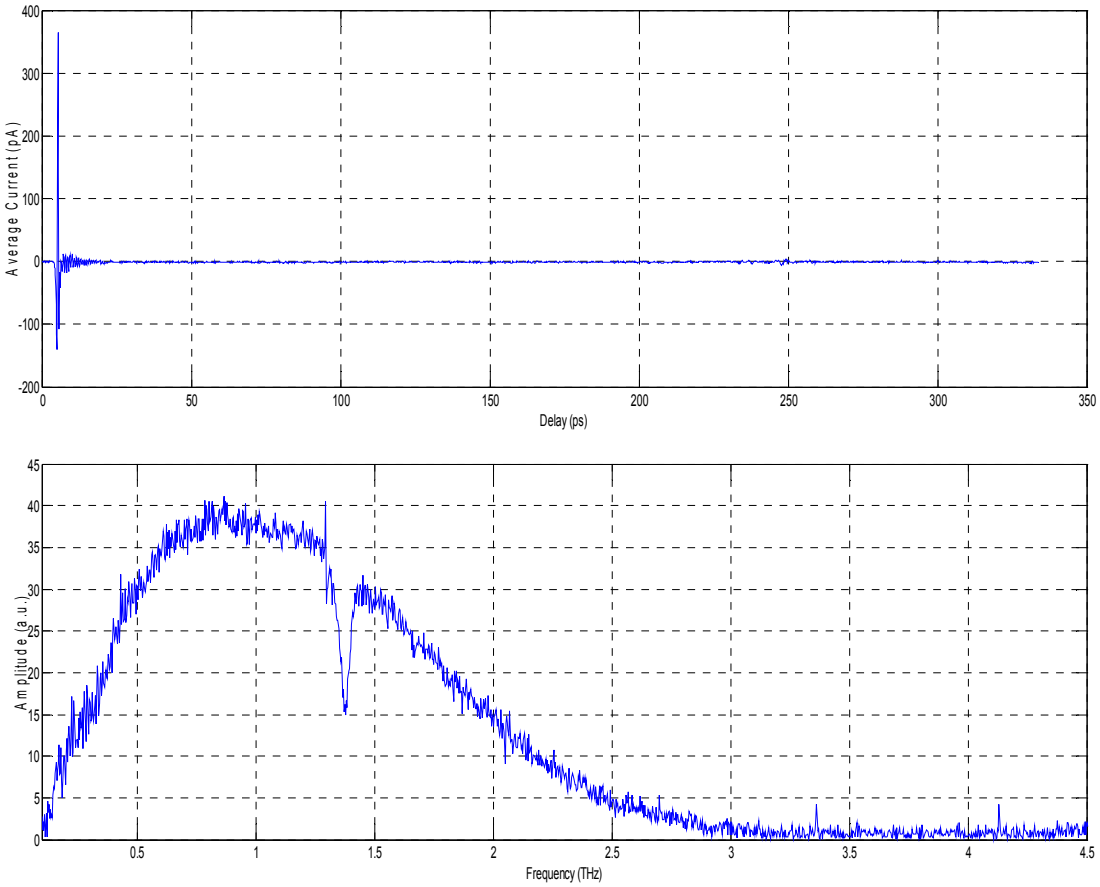

Figure 29: Time domain (top) and resolved frequency domain (bottom) scan from a sample of lactose dropcast onto an aluminum 4ROC CYLWG at room temperature for a long 350 ps scan.

Figure 29 shows a time domain and frequency domain plot of a scan made through the 4ROC CYLWG at room temperature. The scan length was carried out to nearly 350 ps of time using 2500 steps at a 20 μm step size. In this plot, we can see that the reflections normally incurred by the silicon lenses in the quasi-optic method of coupling are not present, and we have now more than doubled the scan length. However, there is a small reflection that occurs at around 250 ps which causes a significant amount of high frequency noise in the plots. This reflection is from the hemispherical silicon lenses that rest on the backsides of the THz transmitter/receiver chips and as such, is systematic and unavoidable. Therefore, we have effectively managed to increase the usable scan length of the system to about 240 ps, or about an extra 100 ps worth of time.

In the room temperature data, only the strongly resonant line at 1.4 THz is evident; the other spectral lines, such as the sharper 0.53 THz resonance, are not evident until the device under test is placed into the cryogenic chiller and cooled to nearly 10K. Figure 30 shows the spectral absorption result from chilling the 4ROC CYLWG with lactose dropcast onto the waveguide. Note that the data shown here has been truncated to 240 ps, cutting off any system reflections. Figure 31 shows the absorption of a chilled quasi-optic PPWG with lactose dropcast onto the waveguide at only 150 ps.

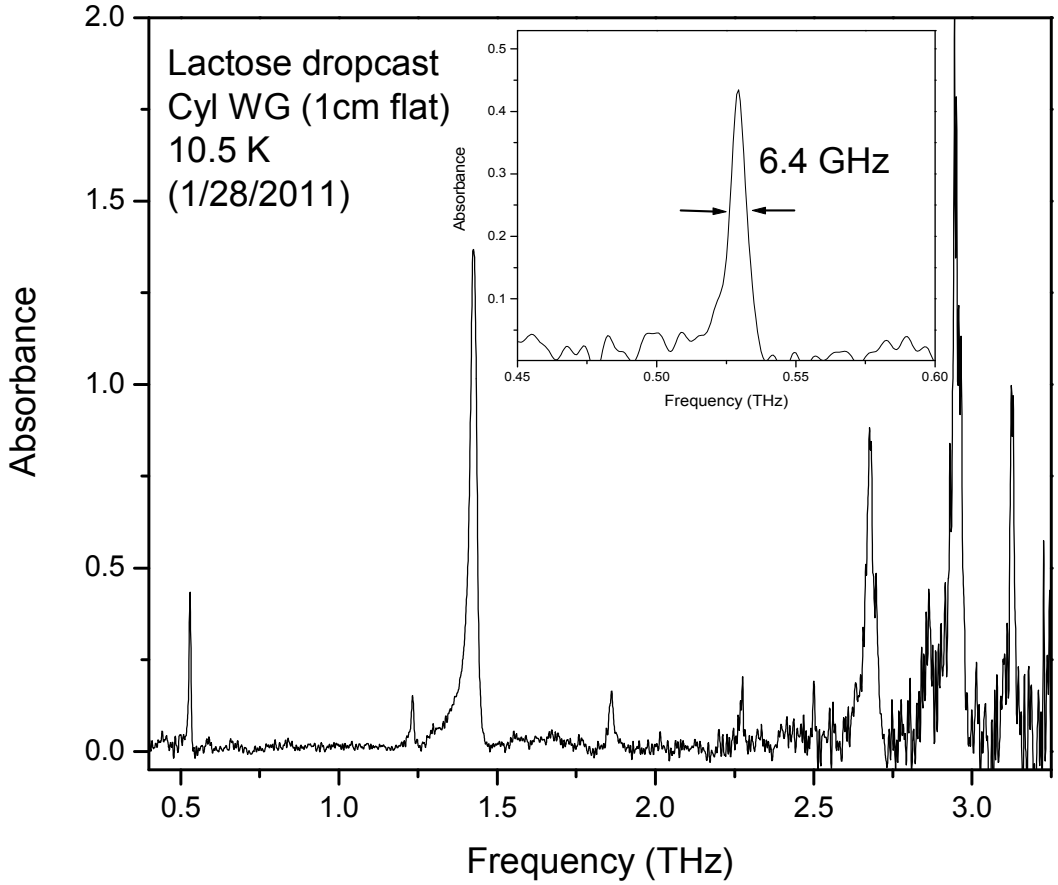

Figure 30: Absorption of lactose dropcast onto the 4ROC CYLWG. The peak at ~ 0.53 THz is one of the narrowest known lines of lactose. Here, the CYLWG has managed to resolve its feature size to 6.4 GHz at FWHM.

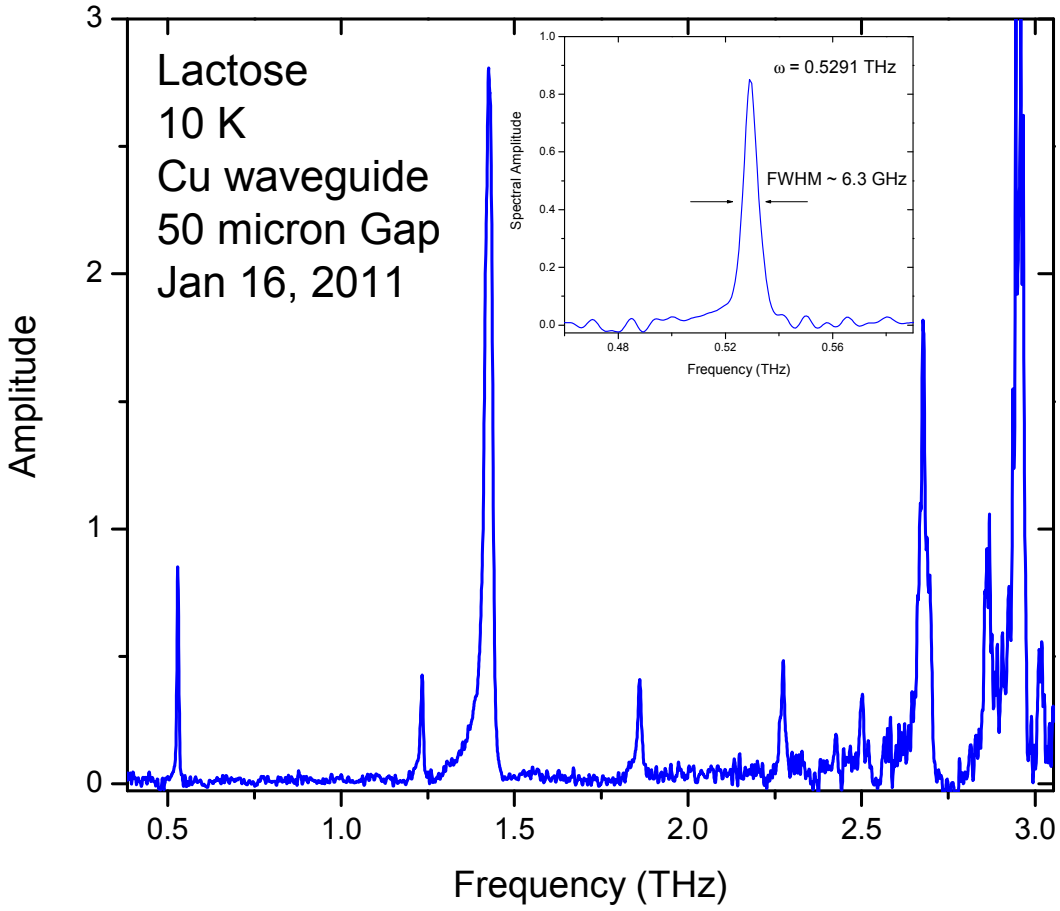

Figure 31: Absorption of lactose deposited onto a silicon-lens coupled PPWG. Compared to the results from the 4ROC CYLWG, this system performed perhaps only marginally better, giving a sharpness of the resonance peak of 6.3 GHz, although the increased performance is perhaps within statistical error [45].

The results between the two waveguides are remarkably comparable. The 4ROC CYLWG was able to resolve the 0.53 THz spectral resonance to 6.4 GHz at FWHM – the quasi-optic PPWG could resolve it to 6.3 GHz, and indeed, the 100 MHz difference between the two is probably well within a reasonable margin of error. More measurements on the CYLWGs may produce exactly equal results. And as seen in Figure 29, the dreaded Fresnel reflections at 150 ps from the quasi-

optic PPWG are gone. The usable scan length of the CYLWG is almost 100 ps longer. Any spectral information that could be obtained by scanning beyond that boundary is now possible.

Unfortunately, for this example we did not find any more spectral information in the longer-scan results. Perhaps with other molecular samples we will see differences, but as for lactose, it is the author's conclusion that spectral data does not exist beyond the 150 ps boundary, so as of yet the question of whether or not the CYLWG will enhance spectroscopic readings is inconclusive.

5. CONCLUSIONS

The use of parallel-plate waveguides for terahertz spectroscopy is becoming more common place. Researchers favor its ease of use and high signal to noise ratio, given its ability to detect strong absorbance features over that of pellets or crystalline samples, and have begun finding other novel ways of exploring their uses within the terahertz regime. However, the matter of coupling has always been an issue. Some have used the quasi-optical technique, noting the limits the silicon places on scan length, while others have merely placed the parallel plates in the terahertz beam waist and hoped for the best. Still others have even explored ways of incorporating horn-like structures onto the plates [15] [16].

The method explored in this work has made simple work of incorporating a gap-independent coupling structure that enhances parallel plate performance to that of the quasi-optical technique while eliminating the limitations imposed by outer silicon lenses. Manufacturing of these waveguides is simple, and incorporation of the parallel plates onto the cylindrical/circular structures introduces no reflections. Further, reproducibility of spectroscopic measurements is enhanced since there are no longer any external or externally-moving components to the setup.

However, there is still more work to be done. As is, these devices need further testing with regards to spectroscopic samples. Initial testing revealed them to be as effective as quasi-optically coupled PPWGs with a lactose sample; however this simple scan is not enough, and more samples should to be tested and re-tested to ensure complete accuracy.

Understanding of the nature of the curvature with regards to coupling and bandwidth would be beneficial. It has been shown that the curve is indeed adiabatic; however, other works have shown that the simple circular curvature of horns can be improved upon, and that incorporating a different taper shape, such as an exponential or sinusoidal curve [38], can enhance coupling throughput. Rigorous mathematical and or numerical analytic models would help to understand how this circular curvature functions and would aid in the design of a better curve. Then the new curve could be incorporated into a different kind of free standing waveguide, one not necessarily manufactured from a metal cylinder, but fully machined out of a plate of metal and shaped into the necessary form, which would not require much more fabrication.

The use of a (near) lossless transmission mode will factor heavily into the future of terahertz research and communications. As we all know, free radiation of terahertz signals is heavily curtailed by the high absorbance of water found in our atmosphere. Despite evidence that suggests that we can still emit, send, and receive signals within certain atmospheric "windows," or ranges in the terahertz frequency spectrum where water does not heavily absorb the radiation [2] [4], by fully encasing the terahertz signal within a medium and radiating along a two-conductor structure, we can greatly preserve the terahertz signal across a much broader spectral range, enhancing the capacity of information that can be carried by such a signal. This is where I see the future of terahertz communications and spectroscopy headed: into a world with flexible, dual-conductor lines that will gradually allow researchers to construct ever more complex and robust terahertz systems.

6. REFERENCES

[1] M. V. Exter and D. R. Grischkowsky, "Characterization of an Optoelectronic Terahertz Beam System," *IEEE Transactions on Microwave Theory and Techniques,* vol. 38, no. 11, pp. 1684-1691, 1990.

[2] Y. Yang, M. Mandehgar and D. Grischkowsky, "Time Domain Measurement of the THz Refractivity of Water Vapor," *Optics Express,* vol. 20, no. 24, pp. 26208-26218, 2012.

[3] J. C. G. Lesurf, "Beam coupling, lenses, and mmirrors," in *Millimetre-Wave Optics, Devices and Systems*, Bristol, Adam Hilger, 1990, pp. 11-28.

[4] Y. Yang, M. Mandehgar and D. R. Grischkowsky, "Understanding THz Pulse Propagation in the Atmosphere," *IEEE Transactions on Terahertz Science and Technology,* vol. 2, no. 406-415, 2012.

[5] R. Mendis and D. Grischkowsky, "Undistorted guided-wave propagation of subpicosecond terahertz pulses," *Optics Letters,* vol. 26, no. 11, pp. 846-848, 2001.

[6] J. Melinger, N. Laman, S. S. Harsha and D. Grischkowsky, "Line narrowing of terahertz vibrational modes for organic thin polycrystalline films within a parallel plate waveguide," *Applied Physics Letters,* vol. 89, pp. 251110-3, 2006.

[7] N. Laman, S. S. Harsha, D. Grischkowsky and J. S. Melinger, "7 GHz resolution waveguide THz spectroscopy of explosives related solids showing new features," *Optics Express,* vol. 16, no. 6, pp. 4094-4105, 2008.

[8] G. Gallot, S. Jamison, R. McGowan and D. Grischkowsky, "THz Waveguides," *Journal of Optical Society of America B,* vol. 17, no. 5, pp. 851-863, 2000.

[9] R. Mendis and D. Grischkowsky, "Plastic Ribbon THz Waveguides," *Journal of Applied Physics,* vol. 88, no. 7, pp. 4449-4451, 2000.

[10] S. Jamison, R. McGowan and D. Grischkowsky, "Single-mode waveguide propagation and reshaping of sub-ps terahertz pulses in sapphire fibers," *Applied Physics Letters,* vol. 76, no. 15, pp. 1987-1989, 2000.

[11] J. Zhang and D. Grischkowsky, "Adiabatic compression of parallel-plate waveguides for sensitivity enchancement of waveguide THz time-domain spectroscopy," *Applied Physics Letters,* vol. 86, p. 061109, 2005.

[12] A. Shutler and D. Grischkowsky, "Gap independent coupling into parallel plate terahertz waveguides using cylindrical horn antennas," *Journal of Applied Physics,* vol. 112, pp. 073102-5, 2012.

[13] N. Marcuvitz, Waveguide Handbook, New York: McGraw-Hill, 1951.

[14] S. S. Harsha, *Engineering Metal Parallel Plate Waveguides as a 2-D Plane for High Resolution THz Time Domain Spectroscopy,* Stillwater, OK: Ph.D. Dissertation, Department of Electrical Engineering, Oklahoma State University, 2011.

[15] W. Mainuelt et. al., "Metal-metal terzhertaz quantum cascade laser with micro-transverse-electromagnetic-horn antenna," *Applied Physics Letters,* vol. 93, no. 183508, 2008.

[16] S.-H. Kim, E. S. Lee, Y. B. Ji and T.-I. Jeon, "Improvement of THz coupling using a tapered parallel-plate waveguide," *Optics Express,* vol. 18, no. 2, pp. 1289-1295, 2010.

[17] M. Theuer, R. Beigang and D. Grischkowsky, "Sensitivity increase for coating thickness determination using THz waveguides," *Optics Express,* vol. 18, no. 11, pp. 11456-11463, 2010.

[18] M. Theuer, R. Beigang and D. Grischkowsky, "Adiabatic Compression of THz Waves Using Metal Flares," *Applied Physics Letters,* vol. 96, no. 191110, 2010.

[19] M. Theuer, S. S. Harsha, R. Beigang and D. Grischkowsky, "Flare coupled metal parallel-plate waveguides for high resolution THz time-domain spectroscopy," *Journal of Applied Physics,* vol. 108, no. 113105, 2010.

[20] R. Mendis and D. Mittleman, "Multifaceted terahertz applications of parallel-plate waveguide: TE1 mode," *Electronics Letters,* vol. 46, no. 26, pp. S40-S44, 2010.

[21] M. Theuer, A. J. Shutler, S. S. Harsha, R. Beigang and D. Grischkowsky, "Terahertz two-cylinder waveguide coupler for transverse-magnetic and transverse-electric mode operation," *Applied Physics Letters,* vol. 98, pp. 0711081-3, 2011.

[22] D. Comparat, "General conditions for quantum adiabatic evolution," Laboratoire Aime Cotton, CNRS, University of Paris-Sud, 2009.

[23] K. J. Laidler, "The meaning of adiabatic," *Canadian Journal of Chemistry,* vol. 72, no. 3, 1994.

[24] M. Amin, "Consistency of the adiabatic theorem," *Physics Review Letters,* vol. 102, no. 22, 2009.

[25] M. Berry, "The adiabatic limit and the semiclassical limit," *Journal of Physics A,* vol. 17, pp. 1225-1233, 1984.

[26] J. D. Love and e. al., "Tapered single-mode fibres and devices, part 1: Adiabaticity criteria," *IEE Proceedings J.,* vol. 138, no. 5, pp. 343 - 354, 1991.

[27] A. R. Mallahzadeh and F. Karshenas, "Modified TEM Horn Antenna for Broadband Applications," *Progress in Electromagnetics Research,* vol. 90, pp. 105-119, 2009.

[28] R. T. Lee and G. S. Smith, "On the characteristic impedance of the TEM horn antenna," *IEEE Transactions on Antennas and Propagation,* vol. 52, no. 1, pp. 315-318, 2004.

[29] W. K. Burns, A. F. Milton and A. Lee, "Optical waveguide parabolic coupling horns," *Applied Physics Letters,* vol. 30, no. 28, 1977.

[30] A. F. Milton and W. K. Burns, "Mode coupling in optical waveguide horns," *IEEE Journal of Quantum Electronics,* Vols. QE-13, no. 10, 1977.

[31] K. Matsumaru, "Reflection Coefficient of E-Plane Tapered Waveguides," *IRE Transactions on Microwave Theory and Techniques,* vol. 6, no. 2, pp. 143-149, 1958.

[32] K. Hongo, "Diffraction by a flanged parallel-plate waveguide," *Radio Science,* vol. 7, no. 10, pp. 955-963, 1972.

[33] K. Hongo and Y. Ogawa, "Receiving characteristics of a flanged parallel-plate waveguide," *IEEE Transactions on Antennas and Propagation,* vol. 25, no. 3, pp. 424-425, 1977.

[34] K. Hongo, Y. Ogawa, T. Itoh and K. Ogusu, "Field distribution in a flanged parallel-plate waveguide," *IEEE Transactions on Antennas and Propagation,* Vols. AP-23, pp. 558-560, 1975.

[35] S. W. Lee, "Ray theory of diffraction by open ended waveguides. I. Field in waveguides.," *Journal of Mathematical Physics,* vol. 11, no. 9, pp. 2830-2850, 1970.

[36] L. Brillouin, "Broad Band Antenna". U.S.A. Patent 2,454,766, 03 November 1948.

[37] A. Nishida, H. Kashiwazaki, S. Yoshida, T. Higashiguchi, N. Yugami and R. Kodama, "A tapered parallel plate waveguide for frequency up conversion of terahertz radiation," *Review of Scientific Instruments,* vol. 83, p. 045104, 2012.

[38] H.-G. Unger, "A Circular Waveguide Taper of Improved Design," *Bell System Technical Journal,* vol. 37, no. 4, pp. 877-898, 1958.

[39] N. Laman and D. Grischkowsky, "Reduced conductivity in the terahertz skin-depth layer of metals," *Applied Physics Letters,* vol. 90, p. 122115, 2007.

[40] S. Ramo, J. Whinnery and T. van-Duzer, in *Fields and Waves in Communications Electronics*, New York, John Wiley and Sons, Inc., 1994, p. 408.

[41] W. Gallagher, C.-C. Chi, I. Duling III, D. Grischkowsky, N. Halas, M. Ketchen and A.

Kleinsasser, "Subpicosecond optoelectronic study of resistive and superconductive transmission lines," *Applied Physics Letters,* vol. 50, pp. 350-353, 1987.

[42] Y. Zhao and D. Grischkowsky, "2-D THz metallic photonic crystals in parallel plate waveguides," *IEEE Transactions on Microwave Theory and Techniques,* vol. 55, pp. 656-663, 2007.

[43] N. L. a. D. Grischkowsky, "Reduced conductivity in the terahertz skin-depth layer of metals," *Applied Physics Letters,* vol. 90, no. 122115, 2007.

[44] N. Laman, S. S. Harsha, D. Grischkowsky and J. S. Melinger, "7 GHz resolution waveguide THz spectroscopy of explosives related solids showing new features," *Optics Express,* vol. 16, no. 6, pp. 4094-4105, 2008.

[45] S. S. Harsha, *Private Communication,* 2012.

VITA

Alisha Shutler

Candidate for the Degree of

Master of Science

Thesis: CIRCULAR WAVEGUIDE TAPERS FOR HIGH RESOLUTION TERZHERTZ SPECTROSCOPY

Major Field: Electrical Engineering

Education:

Completed the requirements for the Master of Science in Electrical Engineering at Oklahoma State University, Stillwater, Oklahoma in July 2016.

Completed the requirements for the Bachelor of Science in Electrical Engineering at Oklahoma State University, Stillwater, Oklahoma in 2009.

Selected Publications:

Alisha J. Shutler and D. Grischkowsky , "Gap independent coupling into parallel plate terahertz waveguides using cylindrical horn antennas," Journal of Applied Physics, Vol. 112, 073102-5 (2012)

Yuping Yang, S. Sree Harsha, Alisha J. Shutler, and Daniel R. Grischkowsky, "Identification of Genestein and Biochanin A. by THz (far-infrared) vibrational spectra," Journal of Pharmaceutical and Biomedical Analysis, *Accepted for publication*, (2012).

Yihong Yang, Alisha Shutler, and D. Grischkowsky, "Measurement of the transmission of the atmosphere from 0.2 to 2 THz ", Optics Express, Vol. 19, 8830-8838, (2011).

M. Theuer, A. J. Shutler, S. Sree Harsha, R. Beigang, and D. Grischkowsky, "Terahertz two-cylinder waveguide coupler for transverse-magnetic and transverse-electric mode operation", Appl. Phys. Lett., Vol. 98, 071108, (2011).